J. Fluid Mech. (2017), *vol.* 820, *pp.* 341–369.
doi:10.1017/jfm.2017.218

Finite Reynolds number effect on the scaling range behaviour of turbulent longitudinal velocity structure functions

S. L. Tang[1,2], R. A. Antonia[3,†], L. Djenidi[3], L. Danaila[4] and Y. Zhou[1,2]

[1]Institute for Turbulence-Noise-Vibration Interaction and Control, Shenzhen Graduate School, Harbin Institute of Technology, Shenzhen, 518055, PR China

[2]Digital Engineering Laboratory of Offshore Equipment, Shenzhen, 518055, PR China

[3]School of Engineering, University of Newcastle, NSW 2308, Australia

[4]CORIA CNRS UMR 6614, Université de Rouen Normandie, 76801 Saint Etienne du Rouvray, France

(Received 10 October 2016; revised 31 March 2017; accepted 2 April 2017; first published online 5 May 2017)

The effect of large-scale forcing on the second- and third-order longitudinal velocity structure functions, evaluated at the Taylor microscale $r = \lambda$, is assessed in various turbulent flows at small to moderate values of the Taylor microscale Reynolds number R_λ. It is found that the contribution of the large-scale terms to the scale by scale energy budget differs from flow to flow. For a fixed R_λ, this contribution is largest on the centreline of a fully developed channel flow but smallest for stationary forced periodic box turbulence. For decaying-type flows, the contribution lies between the previous two cases. Because of the difference in the large-scale term between flows, the third-order longitudinal velocity structure function at $r = \lambda$ differs from flow to flow at small to moderate R_λ. The effect on the second-order velocity structure functions appears to be negligible. More importantly, the effect of R_λ on the scaling range exponent of the longitudinal velocity structure function is assessed using measurements of the streamwise velocity fluctuation u, with R_λ in the range 500–1100, on the axis of a plane jet. It is found that the magnitude of the exponent increases as R_λ increases and the rate of increase depends on the order n. The trend of published structure function data on the axes of an axisymmetric jet and a two-dimensional wake confirms this dependence. For a fixed R_λ, the exponent can vary from flow to flow and for a given flow, the larger R_λ is, the closer the exponent is to the value predicted by Kolmogorov (*Dokl. Akad. Nauk SSSR*, vol. 30, 1941*a*, pp. 299–303) (hereafter K41). The major conclusion is that the finite Reynolds number effect, which depends on the flow, needs to be properly accounted for before determining whether corrections to K41, arising from the intermittency of the energy dissipation rate, are needed. We further point out that it is imprudent, if not incorrect, to associate the finite Reynolds number effect with a consequence of the modified similarity hypothesis introduced by Kolmogorov (*J. Fluid Mech.*, vol. 13, 1962, pp. 82–85) (K62); we contend that this association has misled the vast majority of post K62 investigations of the consequences of K62.

Key words: isotropic turbulence, turbulence theory, turbulent flows

† Email address for correspondence: robert.antonia@newcastle.edu.au

1. Introduction

Kolmogorov's transport equation for the second-order moment of the longitudinal velocity increment δu (u, v and w are the velocity fluctuations in the x (streamwise), y (lateral or transverse) and z (spanwise) directions, respectively) (Kolmogorov 1941*b*), derived from the Navier–Stokes equation for homogeneous and isotropic turbulence (HIT) after neglecting the unsteady (or $\partial/\partial t$) term, is given by

$$-\overline{(\delta u)^3} + 6\nu\frac{\partial}{\partial r}\overline{(\delta u)^2} = \frac{4}{5}\overline{\epsilon}r, \tag{1.1}$$

with $\delta u(r) = u(x+r) - u(x)$, where r is the separation between two points in the x direction; $\overline{\epsilon}$ is the mean energy dissipation rate. The overline denotes time averaging. The first term in (1.1) is the third-order structure function which is proportional to the nonlinear transfer of turbulent energy at a scale r, while the second term represents the viscous effect. The term on the right-hand side of (1.1) is proportional to the mean energy dissipation rate $\overline{\epsilon}$ ($=\overline{\epsilon}_{iso} = 15\nu\overline{(\partial u/\partial x)^2}$ if local isotropy is assumed, ν is the kinematic viscosity of the fluid). This equation is of fundamental importance since it is an equilibrium equation between second- and third-order moments. It represents a mean turbulent energy balance for each scale r provided the Reynolds number is sufficiently large and r is small compared with the integral length scale.

In small to moderate Reynolds number flows, this equation is usually not satisfied except perhaps at small r since (1.1) does not contain the effect of the non-homogeneity associated with large scales. An additional term or terms, here identified for simplicity by the symbol $I_u(r)$, which reflects the influence of the large scales and may hence differ from flow to flow, needs to be added to (1.1) (Danaila, Anselmet & Antonia 2002; Danaila, Antonia & Burattini 2004). A generalized form of (1.1) can be expressed as

$$I_u(r) - \overline{(\delta u)^3} + 6\nu\frac{\partial}{\partial r}\overline{(\delta u)^2} = \frac{4}{5}\overline{\epsilon}r, \tag{1.2}$$

which has been tested in various flows, e.g. decaying HIT (e.g. Danaila *et al.* 1999; Antonia *et al.* 2000*b*), along the axis in the far field of an axisymmetric jet flow where the flow satisfies self-preservation (Burattini, Antonia & Danaila 2005*b*; Thiesset, Antonia & Djenidi 2014), along the centreline of a fully developed channel flow (Danaila *et al.* 2001) and stationary forced periodic box turbulence (or SFPBT) (e.g. Fukayama *et al.* 2000). Obviously, equation (1.1) can only be satisfied up to a maximum separation which depends on the Reynolds number. For example, Danaila *et al.* (1999) showed that (1.1) is satisfied only for $r/\eta \leqslant 5$ ($\eta = (\nu^3/\overline{\epsilon})^{1/4}$) for grid turbulence at $R_\lambda = 66$ ($= u'\lambda/\nu$, where $\lambda = u'/(\partial u/\partial x)'$ and a prime denotes a root-mean-square value), suggesting that $I_u(r)$ contributes to (1.1) for $r/\eta > 5$. Since (1.2) allows the dependence of the small-scale motion (SSM) on large-scale effects to be quantified, it is worth exploring and characterizing this dependence, especially in connection with the inertial range (IR). Since the IR is tenable only at very large R_λ, it is more realistic to use the term scaling range (SR) at finite R_λ with the caveat (Qian 1998) that the SR is not the IR. Noting that Antonia & Burattini (2006) showed that very large values of R_λ (of the order of 10^6) are required before the IR is unequivocally established in decaying-type flows, we shall hereafter refer to the SR. The scale by scale energy budget used in Antonia & Burattini (2006) is for decaying HIT.

We recall that the analytical framework introduced by Kolmogorov (1941*a*,*b*), widely known as K41, and its subsequent modification (Kolmogorov 1962) (or K62), which accounts for the so-called 'internal intermittency' effect has had a tremendous impact on turbulence research. A major outcome of the second similarity hypothesis in K41 is the prediction of the famous IR ($\eta \ll r \ll L$; L is the integral length scale)

$$\overline{(\delta u^*)^n} = C_{un} r^{*n/3}, \tag{1.3}$$

where C_{un} are universal (Kolmogorov) constants, the asterisk denoting normalization by the Kolmogorov length scale and/or Kolmogorov velocity scale ($u_K = (\nu\overline{\epsilon})^{1/4}$). A major consequence of K62 is to modify (1.3) so that $\overline{(\delta u^*)^n}$ is now given by

$$\overline{(\delta u^*)^n} \sim r^{*\zeta_{un}}, \tag{1.4}$$

where ζ_{un} may depart from $n/3$ (e.g. Frisch, Sulem & Nelkin 1978; Antonia, Satyaprakash & Hussain 1982*b*; Anselmet *et al.* 1984; She & Leveque 1994; Maurer, Tabeling & Zocchi 1994; Sreenivasan & Antonia 1997).

We need to make it clear from the outset that, like K41, K62 requires $R_\lambda \to \infty$. Since this is never achieved in either experiments or direct numerical simulations (DNS), the finite Reynolds number (FRN) effect needs to be carefully assessed before drawing any definitive conclusions regarding the validity of the anomalous scaling predicted by K62 or, for that matter, the validity of the K41 predictions. When the FRN effect prevails, and an SR exists, $\overline{(\delta u^*)^n}$ can be expressed, over values of r within the SR, as

$$\overline{(\delta u^*)^n} = C_{un}^{FRN} r^{*\alpha_n}, \tag{1.5}$$

where C_{un}^{FRN} and α_n are likely to depend on the type of flow; α_n can only be identified with ζ_{un} when $R_\lambda \to \infty$. We believe that only estimates of α_n, rather than ζ_{un}, have been made prior to approximately 1997 (e.g. Antonia *et al.* 1982*b*; Anselmet *et al.* 1984; Maurer *et al.* 1994). Since 1997, there is significant evidence (e.g. L'vov & Procaccia 1995; Qian 1997, 1998, 1999; Lindborg 1999; Pearson & Antonia 2001; Antonia & Burattini 2006; Sagaut & Cambon 2008; Bos *et al.* 2012; Tchoufag, Sagaut & Cambon 2012; Meldi & Sagaut 2013) that particular attention needs to be paid to the FRN effect when assessing the SR scaling exponents of either velocity spectra, e.g. $\phi_u(k_1)$, where k_1 is the one-dimensional wavenumber, pressure spectra, $E_p(k_1)$, or velocity structure functions. For example, Pope (2000) (figure 6.29 in his book) made a compilation of different values of the power-law exponent for $\phi_u(k_1)$ measured in grid turbulence and showed that the K41 $-5/3$ power-law scaling is approached slowly as R_λ increases (see also Mydlarski & Warhaft 1996). Ishihara *et al.* (2016) recently examined the three-dimensional energy spectrum for SFPBT ($R_\lambda = 723 - 2297$) and found that there is a FRN effect on the energy spectrum in the SR. Ni & Xia (2013) examined the prefactors of $\overline{(\delta u)^2}$ and the energy spectrum in the SR for various flows, e.g. in the central region of a cylindrical Rayleigh–Bénard turbulent convection cell, an axisymmetric jet, a turbulent boundary layer and SFPBT over a large range of $R_\lambda (= 55–1450)$. They found that all prefactors of $\overline{(\delta u)^2}$ and spectra in these flows depend on R_λ and the type of flow. Morrison, Vallikivi & Smits (2016) examined $\overline{(\delta u)^3}/(\overline{\epsilon} r)$ and $\overline{(\delta u)^2}/(\overline{\epsilon} r)^{2/3}$ in the SR on the centreline of a turbulent pipe flow for R_λ in the range 249–986. They found that both $\overline{(\delta u)^3}/(\overline{\epsilon} r)$ and $\overline{(\delta u)^2}/(\overline{\epsilon} r)^{2/3}$ depend on R_λ. Antonia *et al.* (2015) have examined the dependence

on R_λ of $S_{\delta u}$, the skewness of δu, *viz.* $S_{\delta u} = \overline{(\delta u)^3}/\overline{(\delta u)^2}^{3/2}$, in several turbulent flows. The data indicate that, for $R_\lambda \geqslant 500$, the rate at which $S_{\delta u}$ decreases with increasing r^* diminishes for $r^* \geqslant 20$ but over the SR, $S_{\delta u}$ approaches a constant very slowly, as required by K41. This constancy is still not quite attained at $R_\lambda = 25\,000$ in the eddy-damped quasi-normal Markovian (EDQNM) simulation of decaying HIT of Bos *et al.* (2012). These results reinforce Antonia & Burattini's (2006) finding that, for decaying HIT, R_λ should probably exceed 10^6 before the IR is established unequivocally and Qian's (1997) prediction that R_λ should be higher than 10^4 in order to have an IR wider than one decade. Tsuji & Ishihara (2003) measured pressure spectra ($E_p(k_1)$) on the centreline of a round jet over a large range of R_λ (= 200–1250). They showed that the K41 $-7/3$ power-law scaling for $E_p(k_1)$ is approached as R_λ increases and is confirmed for $R_\lambda \geqslant 600$. Using EDQNM in decaying HIT, Meldi & Sagaut (2013) further confirmed the FRN effect on the pressure spectrum and revealed that $R_\lambda \sim 10\,000$ is needed before the pressure spectrum exhibits an IR with an extension of one decade. However, the FRN effect on the SR scaling exponents of structure functions, especially higher-order structure functions, has yet to be assessed critically either via experiments or DNS. This assessment is the major objective of this paper. We recall here that it is Anselmet *et al.*'s (1984) paper that provided convincing evidence of the anomalous scaling, *viz.* α_n deviates further from the K41 prediction ($n/3$) as n continues to increase. We also want to make it clear that we are not disputing the estimates of α_n obtained by these authors on the axis of a round jet at one value of R_λ (= 835). These estimates have been widely accepted by the turbulence research community and, as we will show later, are appropriate for this particular flow and value of R_λ. Our concern is that the anomalous scaling or departure of α_n from K41, as described by Anselmet *et al.* (1984) and others (e.g. Vincent & Meneguzzi 1991; Sreenivasan & Antonia 1997) have to be reinterpreted in the light of the FRN effect.

This objective is tackled in two parts. In the first (§§ 4 and 5), we try to understand analytically via scale by scale energy budget equations, how $I_u(r)$ affects $\overline{(\delta u^*)^n}$ ($n = 2$ and 3) when $r = \lambda$, a separation which is expected to reside near the lower end of the SR (Antonia, Satyaprakash & Chambers 1982*a*; Danaila *et al.* 2002), in small to moderate R_λ in the turbulent flows mentioned above. We should point out again that a fully developed IR exists when R_λ is very large, if not infinite. When R_λ is not sufficiently large, the SR cannot be identified with IR. Antonia & Burattini (2006) showed clearly that $\overline{(\delta u)^3}/(\overline{\epsilon} r)$ approaches a plateau with a value 4/5, representative of the IR, over an ever expanding range of separations r as R_λ increases, while at the same time both the viscous term and I_u decrease to zero over the same range of separations. They also showed that the maximum of $\overline{(\delta u)^3}/(\overline{\epsilon} r)$ occurs at $r/\lambda \simeq 1$, irrespective of R_λ, thus making our choice $r = \lambda$ a meaningful way of assessing the approach of $\overline{(\delta u)^3}/(\overline{\epsilon} r)$ to the asymptotic value of 4/5. Also, the selection $r = \lambda$ avoids the usual measurement difficulties associated with $r = \eta$; $r = \lambda$ provides therefore a means of quantifying with confidence the influence of $I_u(r)$ on $\overline{(\delta u^*)^n}$. Since $I_u(r)$ is flow dependent, one expects that $\overline{(\delta u^*)^n}$ at $r = \lambda$ may differ among different flows for a fixed value of R_λ.

In the second part (§ 6), the results obtained in the first part are tested against experimental and numerical data for $\overline{(\delta u)^n}$ obtained in several different flows; this is important since the dependence of small-scale statistics on R_λ is inextricably linked, via $I_u(r)$, with that on the nature of the flow (possibly also different initial conditions in the same flow). For example, on the axis of a plane jet, with R_λ in the range

500–1100, where the mean shear is zero, we show that the FRN effect on the SR scaling exponents of $\overline{(\delta u)^n}$ is similar to that experienced by the SR power-law exponents of $\phi_u(k_1)$, $S_{\delta u}$ and $E_p(k)$. We stress that, in this part (§ 6), we focus on the dependence of α_n, as it appears in (1.5), on both R_λ and the type of flow. We believe that this is more appropriate, if not more correct, than simply assigning values of the power-law exponents of $\overline{(\delta u)^n}$ to ζ_{un} (1.4). We believe this practice has led to a major source of confusion in the literature.

The structure of the paper is as follows. The measurements are described briefly in § 2. Local isotropy is examined in § 3. In § 4, we derive a relation, at $r = \lambda$, between $\overline{(\delta u^*)^n}$ and the large-scale term $I_u(r)$ in various turbulent flows. Results obtained in § 4 are tested against experimental and numerical data for $\overline{(\delta u^*)^n}$ obtained in a wide range of flows from small to moderate R_λ; they are presented in § 5. Then, the FRN effect on SR scaling exponents of the longitudinal velocity structure functions at moderately large R_λ (= 500–1100) measured on the axis of a plane jet is discussed and compared with other flows, e.g. circular jet, wake and SFPBT, in § 6. Conclusions are given in § 7.

2. Experimental details

The plane jet used in the present study issues from a two-dimensional contraction of a wind tunnel. Since the experiment was originally carried out by Zhou, Antonia & Chua (2005), a detailed description of the experimental conditions and measurement techniques can be found in that paper. The tunnel comprises a single inlet 15 kW centrifugal fan, which is able to deliver a maximum free stream velocity of approximately 40 m s^{-1}. After the fan outlet, the air enters a settling chamber via a two-stage two-dimensional diffuser. Downstream of the settling chamber (1.6×0.9 m^2), which includes 6 evenly spaced wire-mesh screens and a 5 mm aluminium honey comb, the flow enters a two-dimensional contraction (area ratio is 9.5) and exits in a laminar state. The contraction exit has a height d of 16.5 cm and width $h = 82.5$ cm (aspect ratio is 5). The longitudinal axis of the contraction is 1.2 m above the floor of the laboratory. The main set of measurements was made at a distance $x = 36d$ downstream of the exit, at five values of the exit velocity U_j with a one-component (spanwise) vorticity probe. The magnitude of U_j varies approximately between 8 m s^{-1} and 24 m s^{-1}. Correspondingly, the Reynolds number $R_d = U_j d/\nu$ at the jet exit varies between 8.4×10^4 and 2.6×10^5. The corresponding R_λ range is 500–1100.

The one-component vorticity probe consists of one X-wire lying in the (x, y) plane, straddled by a pair of parallel single hot-wires, each aligned in the z direction. All hot-wires were etched from Wollaston (Pt-10 %Rh) wire to an active length l_w of $200d_w$ (d_w is the wire diameter, here equal to 1.27 μm) to minimize end effects. They were operated with in-house constant temperature anemometers at an overheat ratio of 1.5. Output signals from the anemometers were passed through buck and gain circuits and low-pass filtered at a cutoff frequency f_c close to the Kolmogorov frequency $f_K \equiv U/2\pi\eta$. The filtered signals were sampled (12 bit analogue-to-digital converter) at a frequency f_s set equal to $2f_c$. The record duration was in the range 60–300 s. The separation between the parallel wires Δy is equal to 0.85 mm. For all the Reynolds numbers considered here, l_w/η lies between 1 and 2.4 whilst $\Delta y/\eta$ is in the range 3.5–7.7. The main flow parameters are given in table 1. Note that the uncertainty in estimating λ is less than 4 % for all R_λ in table 1, which gives us confidence that the position of λ has been estimated with sufficient accuracy. It

U_j (m s^{-1})	U (m s^{-1})	u' (m s^{-1})	$\overline{\epsilon}_{iso}$ (m^2 s^{-3})	λ (mm)	Error for λ (%)	η (mm)	f_K (kHz)	f_s (kHz)	R_λ	l_w/η	$\Delta y/\eta$
7.66	2.96	0.74	1.00	11.12	1.0	0.24	1.95	5	550	1.00	3.54
11.63	4.77	1.14	3.46	9.51	1.6	0.18	4.30	8	696	1.39	4.72
14.52	6.60	1.58	9.20	7.82	2.9	0.14	7.60	16	826	1.78	6.07
19.57	8.23	1.95	17.12	7.05	3.2	0.12	11.05	20	914	2.08	7.08
23.54	10.00	2.35	26.78	6.81	3.8	0.11	15.01	25	1067	2.27	7.73

TABLE 1. Flow parameters on the axis of the plane jet.

will be seen later (figures 8–11) that λ is located near the lower end of the SR. The same observation can be also made from figures 1–7 of Gotoh & Nakano (2003) for SFPBT at $R_\lambda = 460$. Note that R_λ (= 500–1100) in table 1 is larger than that of Gotoh & Nakano (2003). On the other hand, the ratio λ/η is in the range 46–62, which is sufficiently large to support the choice of $r = \lambda$, as discussed in the introduction.

3. Local isotropy

A key assumption of K41 and K62 is that small-scale turbulence at sufficiently high R_λ is statistically independent of the large scales. Kolmogorov assumed that the small scales are isotropic in space and stationary in time. Following Monin & Yaglom (2007), a well-known isotropic relation between second-order structure functions of longitudinal and transverse velocity components is given by

$$\overline{(\delta v)^2}_{iso} = \left(1 + \frac{r}{2}\frac{\mathrm{d}}{\mathrm{d}r}\right)\overline{(\delta u)^2}. \tag{3.1}$$

The isotropic relation between third-order structure functions is also given by Monin & Yaglom (2007) (see also (Thiesset, Danaila & Antonia 2013*a*)) as

$$\overline{(\delta u)(\delta v)^2}_{iso} = \left(\frac{1}{6}\frac{\mathrm{d}}{\mathrm{d}r}r\overline{(\delta u)^3}\right). \tag{3.2}$$

Figure 1 shows the ratios between calculated and measured second- and third-order structure functions at $R_\lambda = 550$ and 1067, respectively. For both the second- and third-order structure functions, the departure from local isotropy appears to be relatively small in the dissipation range ($r^* < 20$), the maximum departure being approximately 20 %. In the SR, although there is a systematic departure from local isotropy for both the second- and third-order structure functions, there is also an improvement in local isotropy as R_λ increases. The departure from local isotropy in the SR is reflected by the inequality between β_n ($\overline{(\delta v)^n} \sim r^{\beta_n}$) and α_n (1.5). For example, $\beta_4 = 1.05$, whereas $\alpha_4 \approx 1.34$ at $R_\lambda = 1067$. Note that at $r = \lambda$ figure 1, the departure from local isotropy is within ± 20 % at both the largest and smallest values of R_λ, thus justifying this particular choice of r ($= \lambda$) in the analytical work of next section. We finally recall that the main focus of the present paper is to address the finite Reynolds number effect on the SR behaviour of $\overline{(\delta u)^n}$. Evidently, it would be desirable to further investigate the FRN effect on local isotropy in the SR and the SR behaviour of the transverse structure functions by further increasing R_λ.

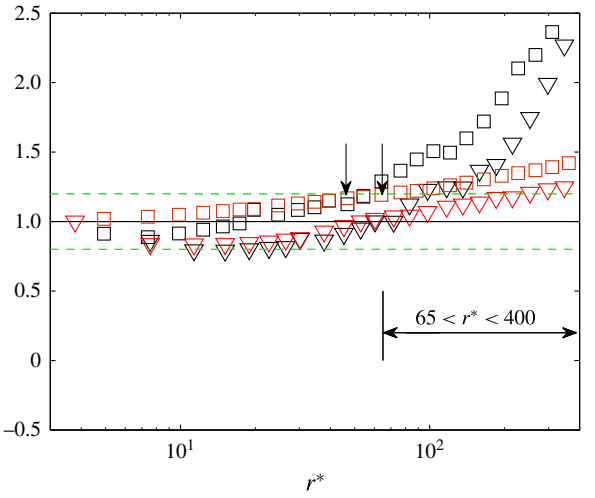

FIGURE 1. (Colour online) Ratios of isotropic and measured second- (red) and third-order (black) structure functions in the dissipation range. ▽, $R_\lambda = 1067$; □, $R_\lambda = 550$. Solid line indicates the isotropic ratio of 1. Dashed green lines indicate a departure of 20 % from the isotropic value of one. Arrowed horizontal line indicates the extent of the scaling range. The vertical arrows indicate the magnitudes of the Taylor microscale (λ/η) at $R_\lambda = 550$ (left) and 1067 (right) respectively.

4. Effect of $I_u(r)$ on $\overline{(\delta u^*)^3}$ at $r = \lambda$

We first discuss the different forms of the term $I_u(r)$ in (1.2) in different types of flows.

(i) In decaying HIT, $I_u(r)$ is the streamwise advection term for $\overline{(\delta u)^2}$ and is given by (e.g. Danaila *et al.* 1999; Antonia *et al.* 2000*b*; Danaila *et al.* 2002, 2004)

$$I_u(r) = -\frac{3}{r^4}\int_0^r s^4 \left[U\frac{\partial \overline{(\delta u)^2}}{\partial x}\right] \mathrm{d}s, \tag{4.1}$$

where s is a dummy variable, identifiable with the separation along x and U is the (constant) mean velocity in the x direction.

(ii) Along the axis in the far field of an axisymmetric jet flow where the flow satisfies self-preservation, $I_u(r)$, which includes a streamwise advection term for $\overline{(\delta u)^2}$ and a production term, is given by (Burattini *et al.* 2005*b*; Thiesset *et al.* 2014)

$$I_u(r) = -\frac{3}{r^4}\int_0^r s^4 \left[U\frac{\partial \overline{(\delta u)^2}}{\partial x} + 2\left[\overline{(\delta u)^2} - \overline{(\delta v)^2}\right]\frac{\partial U}{\partial x}\right] \mathrm{d}s. \tag{4.2}$$

(iii) Along the centreline of a fully developed channel flow, $I_u(r)$, which arises from the turbulent transport of $(\delta u)^2$ by the wall-normal velocity fluctuation v, is given by (Danaila *et al.* 2001)

$$I_u(r) = -\frac{6}{r^4}\int_0^r s^4 \left[\frac{\partial \overline{v(\delta u)^2}}{\partial y}\right] \mathrm{d}s. \tag{4.3}$$

(iv) For SFPBT, the forcing is usually concentrated at very low wavenumbers (i.e. very large scales). For example, $I_u(r)$ is given by (Fukayama *et al.* 2000)

$$I_u(r) = \tfrac{2}{21}\epsilon_{in}(k_e r)^2 r, \tag{4.4}$$

where ϵ_{in} is the energy input rate due to external random forces concentrated at wavenumber $k \sim k_e$.

The scale by scale energy budget equations, with the various forms of I_u, have already been satisfactorily validated over the range $\eta \leqslant r \leqslant L$ against experimental and numerical data in various turbulent flows. This has been reported for grid turbulence (Danaila *et al.* 1999; Antonia *et al.* 2000*b*; Danaila *et al.* 2002, 2004; Antonia & Burattini 2006), along the axis in the far field of an axisymmetric jet flow (Danaila *et al.* 2004; Burattini, Antonia & Danaila 2005*a*), along the centreline of a fully developed channel flow (Danaila *et al.* 2001, 2002; Fukayama *et al.* 2000). For this reason, and to limit the length of this present paper, we only focus on the variation of $I_u(r)$ at $r = \lambda$ on R_λ.

After dividing by u_K^3 and taking $r = \lambda$, the term on the right-hand side of (1.2) becomes

$$\frac{4}{5u_K^3}\overline{\epsilon} r = \frac{4}{5}\lambda^*, \tag{4.5}$$

while the second and third terms on the left-hand side of (1.2) become

$$-\left.\frac{\overline{(\delta u)^3}}{u_K^3}\right|_{r=\lambda} = T_\lambda, \tag{4.6}$$

$$\frac{6\nu}{u_K^3}\frac{\partial\overline{(\delta u)^2}}{\partial r} = 6\left.\frac{\partial\overline{(\delta u^*)^2}}{\partial r^*}\right|_{r=\lambda} = V_\lambda. \tag{4.7}$$

After normalizing by Kolmogorov scales and taking $r = \lambda$, $I_u(r)$ can be written, for decaying HIT, as

$$I_u(\lambda^*) = -\frac{3}{\lambda^{*4}}\int_0^{\lambda^*} s^{*4}\left[U^*\frac{\partial\overline{(\delta u^*)^2}}{\partial x^*}\right]\mathrm{d}s^*. \tag{4.8}$$

$I_u(\lambda^*)$ is not written here for other flows since it is simply the normalized form of (4.2)–(4.4).

It is worth recalling that, by assuming self-preservation for decaying HIT, $I_u(\lambda^*)$ can also be recast as

$$I_u(\lambda^*) = \frac{\sqrt{15}}{2}\left(\frac{n-1}{n}\right)\left(\int_0^{\lambda^*} s^{*5}\frac{\partial\overline{(\delta u^*)^2}}{\partial r^*}\,\mathrm{d}s^* + 2\int_0^{\lambda^*} s^{*4}\overline{(\delta u^*)^2}\,\mathrm{d}s^*\right)\frac{1}{\lambda^{*4}R_\lambda}, \tag{4.9}$$

where n is the power-law decay rate for $\overline{u^2}$, *viz.* $\overline{u^2} \sim x^{-n}$. Strictly, complete self-preservation or self-preservation at all scales is tenable in decaying HIT only when $R_\lambda \to \infty$ (Djenidi & Antonia 2015). However, similarity based on Kolmogorov scales should be applicable in some regions of any turbulent flow when r is sufficiently small, e.g. Antonia, Djenidi & Danaila (2014). This justifies the use of Kolmogorov scales

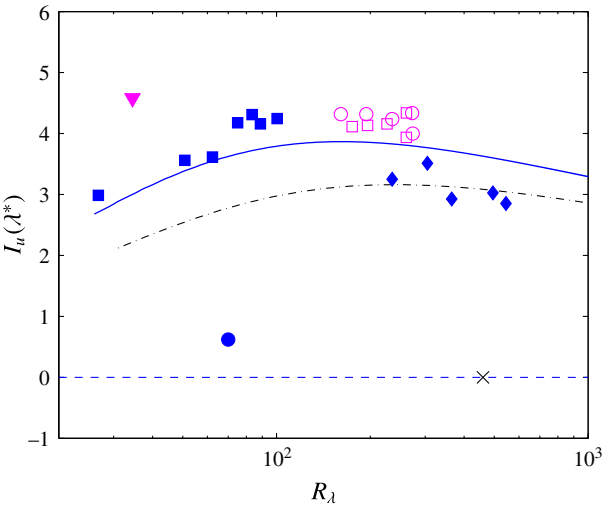

FIGURE 2. (Colour online) Dependence of $I_u(\lambda^*)$ on R_λ in different flows. ■, grid turbulence (Zhou & Antonia 2000); ○ and □ correspond to the data in circular and square cylinder wakes respectively (Antonia, Zhou & Romano 2002*b*); SFPBT: ●, (Fukayama *et al.* 2000); ×, (Gotoh, Fukayama & Nakano 2002); ▼, channel centreline (Danaila *et al.* 2001); ◆, circular jet axis, estimates from the data of Xu, Antonia & Rajagopalan (2001). The solid and dash-dotted curves correspond to the model for decaying HIT (Antonia & Burattini 2006) and jet axis. The horizontal dashed line indicates a value of zero, i.e. the value expected when there is no effect from the large scales.

in (4.9) at $r=\lambda$. Along the axis in the far field of the round jet, $I_u(r^*)$ can be also recast as

$$I_u(\lambda^*)=\left(\frac{3\sqrt{15}}{2+R}\right)R_\lambda^{-1}(\Gamma_1^*+4\Gamma_2^*-2\Gamma_3^*)r^{*-4}, \tag{4.10}$$

where $\Gamma_1^*=\int_0^{r^*}s^{*5}\partial\overline{(\delta u^*)^2}/\partial r^*\mathrm{d}s^*$, $\Gamma_2^*=\int_0^{r^*}s^{*4}\overline{(\delta u^*)^2}\mathrm{d}s^*$, $\Gamma_3^*=\int_0^{r^*}s^{*4}\overline{(\delta v^*)^2}\mathrm{d}s^*$ (see also the first term on the left-hand side of (2.17) in Thiesset *et al.* (2014)), at all scales, not only at $r=\lambda$ since complete self-preservation is satisfied.

Finally, equation (1.2) can be written, when $r=\lambda$, as

$$I_u(\lambda^*)+T_\lambda+V_\lambda=\tfrac{4}{5}\lambda^*, \tag{4.11}$$

where $I_u(\lambda^*)$ differs from flow to flow and possibly from position to position in a given flow. The main objective for deriving (4.11) is to assess the influence of $I_u(\lambda^*)$ on $\overline{(\delta u^*)^n}$ ($n=2$ and 3 at $r=\lambda$, $-\overline{(\delta u^*)^3}_{r=\lambda}=T_\lambda$) in the turbulent flows mentioned above, i.e. decaying HIT, the centreline of a fully developed channel flow, the axis of a turbulent round jet and SFPBT, for as wide a range of R_λ.

5. Results for $\overline{(\delta u^*)^n}$ ($n=2$ and 3 at $r=\lambda$, $-\overline{(\delta u^*)^3}_{r=\lambda}=T_\lambda$)

Estimates of $I_u(\lambda^*)$ for the different flows considered in § 4 have been obtained with experimental and numerical data and are shown in figure 2. Also included are estimates inferred from the parameterized form of $\overline{(\delta u^*)^2}$ in decaying HIT (Kurien &

Sreenivasan 2000; Antonia *et al.* 2003; Antonia & Burattini 2006), *viz.*

$$\overline{(\delta u^*)^2} = \frac{r^{*2}(1+\beta r^*)^{(2c-2)}}{15(1+\alpha r^{*2})^c}, \tag{5.1}$$

where α ($=30^{-3/2}$) is a measure of the cross-over between the dissipative and scaling ranges, $c = 1 - \zeta/2$ ($\zeta = 2/3$ is the scaling range exponent without intermittency correction) and $\beta = L^{*-1}$ (L is the integral length scale). For isotropic turbulence, $\lambda^* = 15^{1/4}R_\lambda^{1/2}$ and $L^* = C_\epsilon 15^{-3/4}R_\lambda^{3/2}$ ($C_\epsilon = 1$ for decaying HIT). Here the correction for ζ is not essential for estimating $I_u(\lambda^*)$, e.g. distributions of $I_u(\lambda^*)$ which correspond to $\zeta = 2/3$ and $\zeta = 0.71$, the value used by Anselmet *et al.* (1984), are almost identical (they are not shown here). This model has been tested in some detail by Antonia & Burattini (2006); they showed that R_λ needs to exceed 10^6 before the IR is established unequivocally. Note that an earlier version of this model was also tested extensively (Antonia, Pearson & Zhou 2002*a*) in other flows. Following Monin & Yaglom (2007), the well-known isotropic relation between $\overline{(\delta u)^2}$ and $\overline{(\delta v)^2}$ is given by (3.1). Relations (5.1) and (3.1) allow $I_u(\lambda^*)$ to be estimated for the flow along the axis of a round jet. All the parameters are chosen to be the same as in decaying HIT except for C_ϵ which is 0.75 (Mi, Xu & Zhou 2013); note that C_ϵ has a negligible effect on the estimate of $I_u(\lambda^*)$. Since the one-point energy budget in the intermediate wake of either a circular cylinder (Thiesset, Antonia & Danaila 2013*b*) or square cylinder (Lefeuvre (2014), private communication) is quite similar to that for decaying HIT, estimates of $I_u(\lambda^*)$ in these two flows at $x/d = 70$, where d is the diameter of the cylinder, are also shown; these values are estimated from the data of Antonia *et al.* (2002*b*).

Figure 2 indicates that $I_u(\lambda^*)$ varies markedly among different flows. For example, it is smallest, if not negligible, for SFPBT, suggesting that this flow is most ideal for examining scaling exponents of $\overline{(\delta u)^3}$ in the scaling range. Indeed, Moisy, Tabeling & Willaime (1999), Antonia & Burattini (2006), Gotoh & Watanabe (2015) showed that $R_\lambda \sim 10^3$ appears to be sufficient for the K41 4/5 law is approached in this flow. Along the centreline of a fully developed channel flow, $I_u(\lambda^*)$ is largest of all cases considered here. For decaying HIT and on the cylinder wake axis, the magnitude of $I_u(\lambda^*)$ is in reasonable agreement with the prediction from the model of (5.1) for decaying HIT. The prediction from the model for the round jet, in good agreement with the magnitude of $I_u(\lambda^*)$ estimated from the data of Xu *et al.* (2001), is smaller than in decaying HIT since an additional production term $I_u(r)$ emerges on the left-hand side of (4.2). In order to show how large a value of R_λ is needed for $I_u(\lambda^*)$ to be negligible, figure 3(*a*) shows the predictions from the models for the round jet and decaying HIT up to $R_\lambda = 10^8$. It is clear from this figure that, for both flows, R_λ should exceed 10^8 for $I_u(\lambda^*)$ to become negligible. For $I_u(\lambda^*)/\lambda^*$ in figure 3(*b*), it approaches zero when $R_\lambda > 10^5$, beyond which the K41 4/5 law is approached (Antonia & Burattini 2006). It is clear that, at $r = \lambda$ (a scale which lies near the start of the SR), the contribution of the large-scale terms to the scale by scale energy budget in decaying-type flows can persist at high R_λ and this contribution is expected to become larger as r increases beyond $r = \lambda$ in the SR. However, it is well known that for laboratory measurements, on the other hand, R_λ hardly ever exceeds 10^3; exceptions are the experiments of Tabeling *et al.* (1996) and Belin *et al.* (1997) who used low temperature helium in a cylindrical container between two counter-rotating disks. In this flow, the maximum value of R_λ reached 5000.

Estimates of V_λ for the flows considered in figure 2 are shown in figure 4. Also included are estimates inferred from (5.1). Since the one-point energy budget along

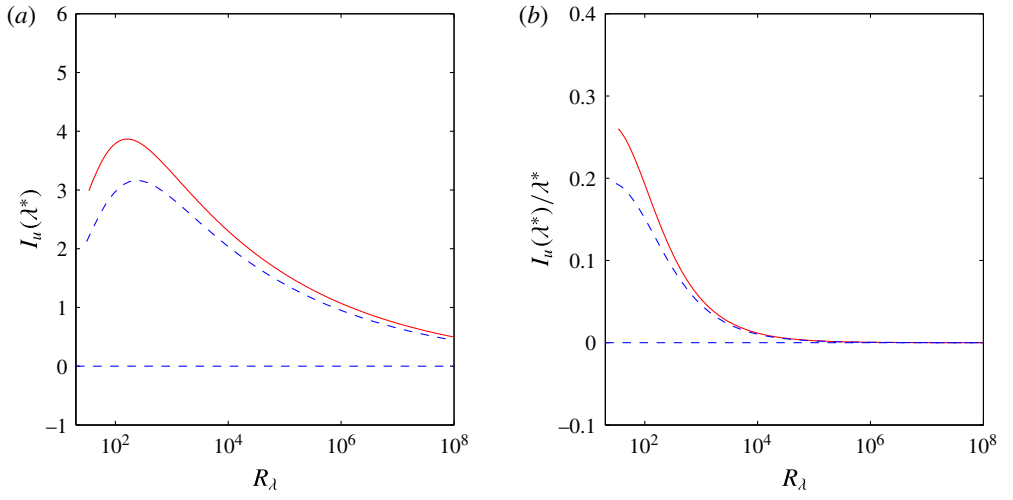

FIGURE 3. (Colour online) Dependence of $I_u(\lambda^*)$ (*a*) and $I_u(\lambda^*)/\lambda^*$ (*b*) on R_λ in decaying HIT (solid curve) and along the axis of a circular jet (dashed curve). Both curves are estimated from the models ((5.1) is introduced in (4.9) to obtain $I_u(\lambda^*)$ in decaying HIT; (5.1) and (3.1) are introduced in (4.10) to obtain $I_u(\lambda^*)$ along the axis of a circular jet). The horizontal dashed line indicates a value of zero, i.e. the value expected when there is no effect from the large scales.

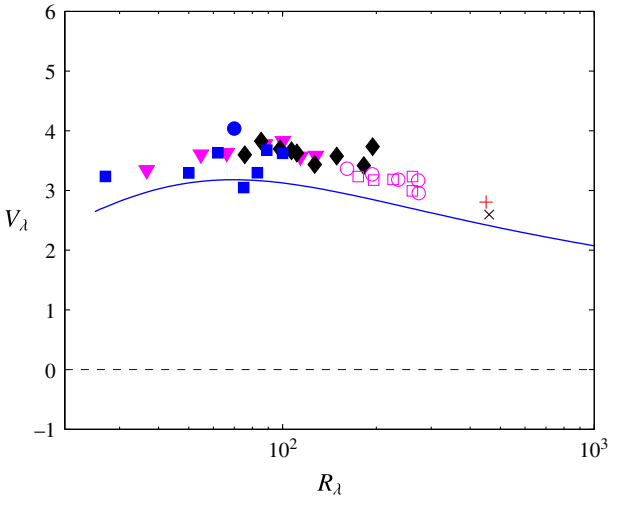

FIGURE 4. (Colour online) Dependence of V_λ, the normalized 'viscous' term in (1.2), on R_λ in different flows. ■, grid turbulence (Zhou & Antonia 2000); ○ and □ correspond to the data in circular and square cylinder wake respectively (Antonia *et al.* 2002*b*); ▼, channel centreline (Tang *et al.* 2015*a*); ◆, pipe axis (Antonia & Pearson 2000); SFPBT: ●, Fukayama *et al.* (2000); ×, Gotoh *et al.* (2002). The solid curve corresponds to the model for decaying HIT (Antonia & Burattini 2006). The horizontal dashed line indicates a value of zero, i.e. the value expected when there is no effect from the small scales.

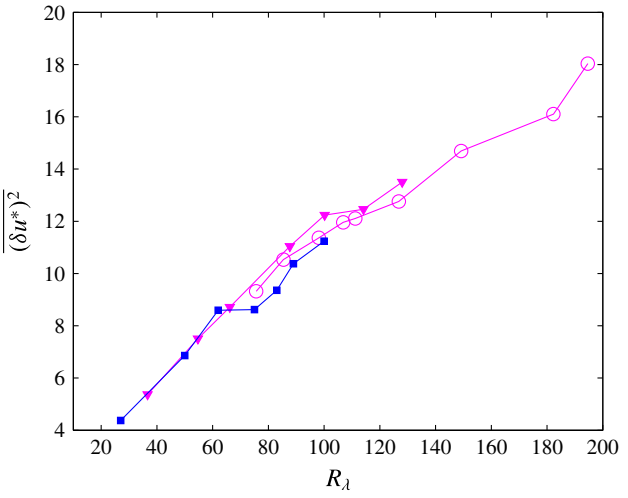

FIGURE 5. (Colour online) R_λ dependence of $\overline{(\delta u^*)^2}$ in different flows at $r = \lambda$. ■, grid turbulence (Zhou & Antonia 2000); ▼, channel centreline (Tang *et al.* 2015*a*); ○, pipe axis (Antonia & Pearson 2000).

the axis of a pipe is quite similar to that on the channel centreline, estimates of V_λ on the axis of the pipe are also shown (Antonia & Pearson 2000). In contrast to $I_u(\lambda^*)$ in figure 2, the values of V_λ (see figure 4) in different flows are closer together and appear to be independent of the flow. However, it is somewhat surprising that, for decaying-type flows, V_λ is close to $I_u(\lambda^*)$ (see figure 2) suggesting that the viscous term and the large-scale term $I_u(\lambda^*)$ have comparable contributions (see also figure 7) to the scale by scale energy budget equation in these flows at $r = \lambda$; this can also be seen from the results of Antonia & Burattini (2006). In SFPBT, the viscous term is significantly larger than the large-scale forcing term $I_u(\lambda^*)$ (i.e. $I_u(\lambda^*) < V_\lambda$) when the external forcing is concentrated at very low wavenumbers (i.e. very large scales). In contrast, on the centreline of a fully developed channel flow, the large-scale term $I_u(\lambda^*)$ makes a larger contribution to the energy budget than the viscous term at low R_λ. Estimates from the model (5.1) collapse reasonably well with the data from grid turbulence over the range $30 < R_\lambda < 100$. In similar manner to $I_u(\lambda^*)$ (figure 2), figure 4 shows that R_λ also needs to be large before V_λ can be neglected, suggesting that the viscous term contributes to the budget at $r = \lambda$ from small to moderate R_λ.

The main message of figure 2 is that, at $r = \lambda$, the contributions from the large-scale forcing term to the scale by scale energy budget equation differ from flow to flow at small to moderate R_λ. Thus, T_λ (see (4.6)) at $r = \lambda$ may also differ from flow to flow at small to moderate R_λ. Although it appears to be independent of the flow, the viscous term has comparable contributions to that of the large-scale term in decaying-type flows. The effect of $I_u(\lambda^*)$ on T_λ and $\overline{(\delta u^*)^2}$ is discussed below.

Figure 5 shows $\overline{(\delta u^*)^2}$ for three of the flows considered in § 4. No data are available at low R_λ for SFPBT and along the jet axis. Also included are estimates inferred from the data measured along the axis of a pipe. It is clear that $\overline{(\delta u^*)^2}$, like the viscous term V_λ (see figure 4), is nearly independent of the flow.

As shown in figures 2 and 4, and although V_λ appears to be independent of the flow, $I_u(\lambda^*)$ differs from flow to flow at small to moderate R_λ. Accordingly, T_λ also differs

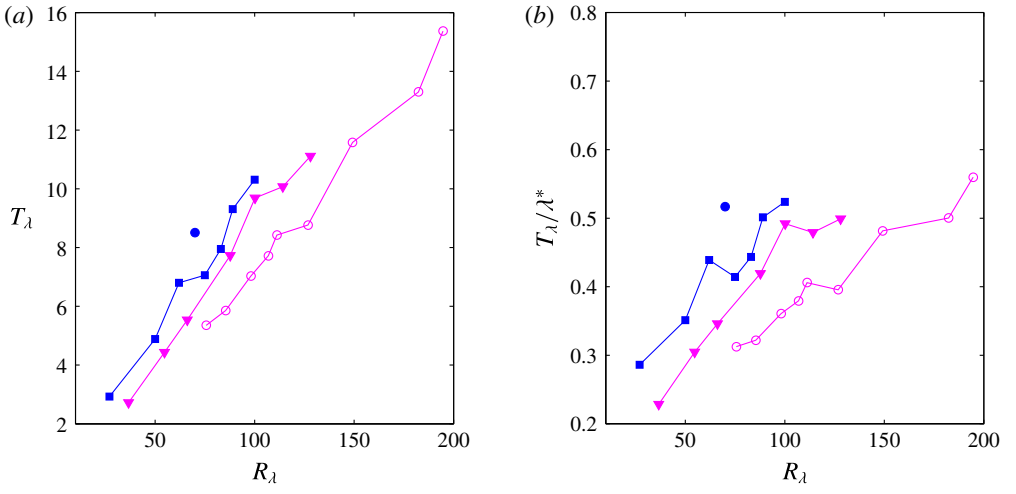

FIGURE 6. (Colour online) (*a*) R_λ dependence of T_λ $(= -\overline{(\delta u^*)^3}|_{r=\lambda})$ in different flows. ■, grid turbulence (Zhou & Antonia 2000); SFPBT: ●, Fukayama *et al.* (2000); ▼, channel centreline (Tang *et al.* 2015*a*); ○, pipe axis (Antonia & Pearson 2000). (*b*) T_λ/λ^* $(= -\overline{(\delta u^*)^3}|_{r=\lambda}/\lambda^*)$ symbols correspond to (*a*).

in different flows over the same range of R_λ. The smallest values of T_λ occur on the axis of the pipe. In decaying grid turbulence, T_λ is larger than along the channel centreline, which is consistent with the smaller values of $I_u(\lambda^*)$ (figure 2) in the former flow. The largest value occurs for SFPBT; this is consistent with the smallest values of $I_u(\lambda^*)$ in figure 2. We should stress that T_λ/λ^* must approach the K41 4/5 law as R_λ continues to increase (Antonia & Burattini 2006) and the way the 4/5 law is approached should become flow dependent as suggested in figure 6(*b*).

In order to highlight the effect of the small scales and the large scales on T_λ/λ^*, the distributions in figures 3(*b*), 4, and 6(*b*) are replotted in figure 7. It can be seen from this figure that T_λ/λ^* must eventually dominate over the other two terms (viscous term and large-scale term) as R_λ becomes large enough. Overall, figure 7 strongly supports the idea that the large-scale forcing (or FRN effect), which differs from flow to flow, has a significant effect on T_λ at small to moderate R_λ. This effect is expected to be amplified as r increases beyond $r = \lambda$ in the SR. It is similar to the FRN effect on the SR power-law exponents of $\phi_u(k_1)$, $S_{\delta u}$ and $E_p(k_1)$ as mentioned in the Introduction. In the next section, we examine the FRN effect on the SR scaling exponents of the longitudinal velocity structure functions at large R_λ $(= 500–1100)$ on the axis of a plane jet.

6. SR scaling exponents of velocity structure functions

In §§ 4 and 5, we have focused on low-order moments because there is an analytical framework, based on (1.2), to describe the relation between $\overline{(\delta u)^2}$ and $\overline{(\delta u)^3}$. This section will focus primarily on the higher-order moments and the SR scaling exponents of $\overline{(\delta u)^n}$. For the higher-order moments, it would be desirable to consider their transport equations which may allow an analytical estimate of the large-scale forcing effect (or FRN effect) on $\overline{(\delta u)^n}$, as is done in §§ 4 and 5 for low-order moments. Although these equations are available, e.g. Hill (2001), evaluating the

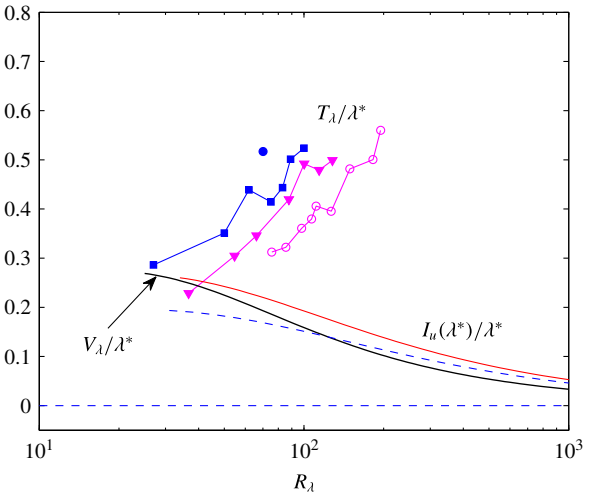

FIGURE 7. (Colour online) Dependence of $I_u(\lambda^*)/\lambda^*$, T_λ/λ^* (the symbols are as in figure 6), and V_λ/λ^* on R_λ in different flows. The horizontal dashed line indicates a value of zero, i.e. the value expected when there is no effect from the small scales and the large scales.

large-scale forcing effect is not straightforward. For example, the equation relating third- and fourth-order moments involve a pressure gradient velocity–velocity structure function, which we are only able to evaluate by making further assumptions. For this reason, we focus in this section on the SR behaviour of $\overline{(\delta u)^n}$ although transport equations for $n > 2$ are outside the scope of this paper.

6.1. *Plane and circular jets*

Figures 8–10 show the fourth-, sixth- and eighth-order structure functions in the scaling range measured on the axis of a plane jet at $R_\lambda = 550$ (red) and 1067 (black), respectively. For clarity, distributions for only two values of R_λ are shown but we emphasize that the variation of $\overline{(\delta u^*)^n}$ with R_λ is systematic for all values of n. In each case, dashed lines are least squares fits across the SR: $60 < r^* < 350$ and $70 < r^* < 400$ for $R_\lambda = 550$ and 1067, respectively. For the purpose of comparison, the SR at each R_λ is fixed ($65 < r^* < 400$, see figure 11). There is a clear R_λ dependence of the scaling exponents for all the fourth-, sixth- and eighth-order structure functions. Figure 11 shows compensated fourth-, sixth- and eighth-order structure functions which correspond to figures 8–10, i.e. $\overline{(\delta u^*)^4} r^{*-1.24}$ and $\overline{(\delta u^*)^4} r^{*-1.34}$ (solid curves), $\overline{(\delta u^*)^6} r^{*-1.66}$ and $\overline{(\delta u^*)^6} r^{*-1.87}$ (dashed curves), $\overline{(\delta u^*)^8} r^{*-1.95}$ and $\overline{(\delta u^*)^8} r^{*-2.45}$ (dash-dotted curves). It can be seen from this figure that all distributions exhibit an approximate plateau in the SR, thus confirming the R_λ dependence of the scaling exponents for all the 4th, 6th and 8th-order structure functions shown in figures 8–10. Also included in figure 11 are the distributions of $\overline{(\delta u^*)^2} r^{*-2/3}$ and $\overline{(\delta u^*)^3} r^{*-\alpha_3}$ ($\alpha_3 = 0.94$ and 1) at $R_\lambda = 550$ and 1067, respectively. As expected, the SR value for $\overline{(\delta u^*)^3}$ approaches 4/5 (K41) as R_λ increases. $\overline{(\delta u^*)^2} r^{*-2/3}$ also exhibits an approximate plateau (both for the present data and the data of Anselmet *et al.* (1984)) on the axis of a circular jet, suggesting a R_λ independence of the exponent for $\overline{(\delta u^*)^2}$ over the

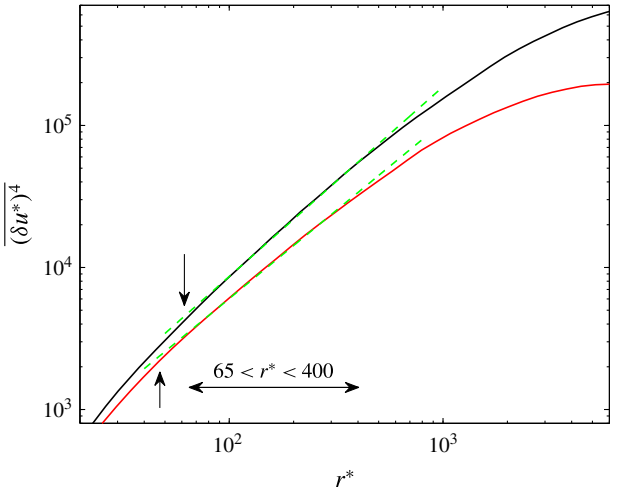

FIGURE 8. (Colour online) Fourth-order structure functions for $R_\lambda = 550$ (red) and 1067 (black). Dashed lines ($\sim r^{*1.24}$ and $\sim r^{*1.34}$) are least squares fits over the SR, corresponding to $R_\lambda = 550$ (red) and 1067 (black) respectively. The arrowed horizontal line indicates the extent of the SR. The vertical arrows indicate the magnitudes of the Taylor microscale (λ/η) at $R_\lambda = 550$ (upward arrow) and 1067 (downward arrow) respectively.

present R_λ range. Note that the value of 2/3 has been obtained by the same method used to determine all the other exponents α_n, i.e. by visually choosing the value of α_2 which gives the 'best' plateau when plotting $\overline{(\delta u^*)^2} r^{*-\alpha_2}$ versus r^*. A slightly larger magnitude (≈ 0.7), constant over this range of R_λ, was estimated by Antonia, Pearson & Zhou (2000*a*) using the same plane jet data after fitting the measured values of $\overline{(\delta u)^2}$ to the relation for $\overline{(\delta u)^2}$ developed by Batchelor (1951), *viz.* equation (4.1) with $\beta = 0$, to describe both the dissipative and scaling ranges. Clearly, the magnitude of α_2 shows a sensitivity to the method used for its determination. With the present method, there is no collapse in the SR (figure 11), suggesting that the Kolmogorov constant C_K ($\overline{(\delta u^*)^2} = C_K r^{*2/3}$) has not yet been attained by the data. Note that the FRN effect on the low-order moments of $\overline{(\delta u^*)^n}$ is consistent with the observations by Pearson & Antonia (2001) over a large range of R_λ ($40 < R_\lambda < 4250$). Although not shown here, the R_λ dependence of the SR exponents for the fifth- and seventh-order structure functions is also observed. This underlines that the FRN effect across the SR must be assessed carefully before attempting to test either K41 or K62.

Figure 13, which illustrates the dependence of α_4 on R_λ, shows that α_4 continues to increase as R_λ increases and eventually seems to approach a constant value, which is close to 4/3, the prediction of K41 ((1.3) with $n = 4$). Evidently, even larger values of R_λ are required to establish this unequivocally. We recall here that the fourth-order velocity structure functions in isotropic turbulence can be written solely in terms of the pressure structure function (derived from the Navier–Stokes equation) (Hill & Wilczak 1995; Vedula & Yeung 1999; Pearson & Antonia 2001)

$$D_p(r) = -\frac{1}{3}D_{1111}(r) + \frac{4}{3}r^2 \int_r^\infty y^{-3}[D_{1111}(y) + D_{\chi\chi\chi\chi}(y) - 6D_{11\gamma\gamma}(y)]\,\mathrm{d}y \times \frac{4}{3}\int_0^r y^{-1}[D_{\chi\chi\chi\chi}(y) - 3D_{11\gamma\gamma}(y)]\,\mathrm{d}y, \tag{6.1}$$

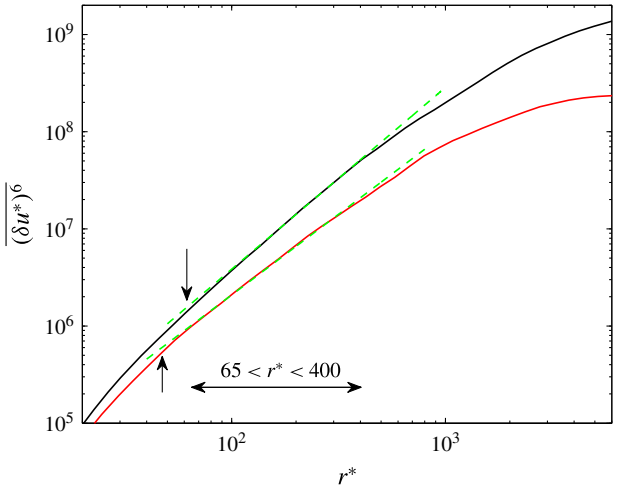

FIGURE 9. (Colour online) Sixth-order structure functions for $R_\lambda = 550$ (red) and 1067 (black). Dashed lines ($\sim r^{*1.66}$ and $\sim r^{*1.87}$) are least squares fits over the SR, corresponding to $R_\lambda = 550$ (red) and 1067 (black) respectively. The arrowed horizontal line indicates the extent of the SR. The vertical arrows indicate the magnitudes of the Taylor microscale (λ/η) at $R_\lambda = 550$ (upward arrow) and 1067 (downward arrow) respectively.

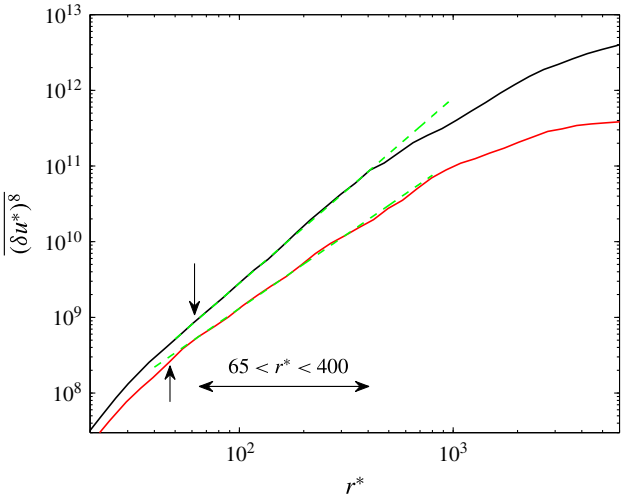

FIGURE 10. (Colour online) Eighth-order structure functions for $R_\lambda = 550$ (red) and 1067 (black). Dashed lines ($\sim r^{*1.95}$ and $\sim r^{*2.45}$) are least squares fits over the SR, corresponding to $R_\lambda = 550$ (red) and 1067 (black) respectively. The arrowed horizontal line indicates the extent of the SR. The vertical arrows indicate the magnitudes of the Taylor microscale (λ/η) at $R_\lambda = 550$ (upward arrow) and 1067 (downward arrow) respectively.

where $D_p(r)$ is the pressure structure function, $D_{1111}(r)$ $(= \overline{(\delta u)^4})$ is the fourth-order longitudinal velocity structure function, χ and γ stand for 2 or 3. The only assumption for deriving (6.1) is that the turbulence is locally homogeneous and isotropic. Equation (6.1) indicates that, in the SR, if $D_{1111}(r)$ varies like $r^{4/3}$, $D_p(r)$ should also vary like

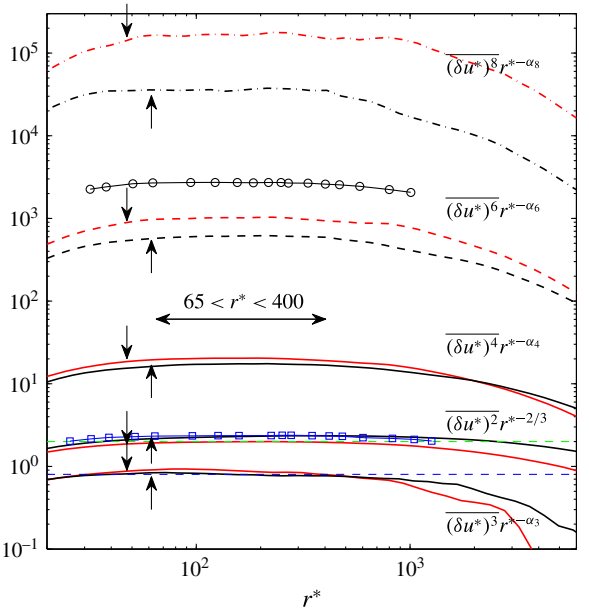

FIGURE 11. (Colour online) Compensated structure functions which correspond to figures 8 ($\alpha_4 = 1.24$ and 1.34), 9 ($\alpha_6 = 1.66$ and 1.87) and 10 ($\alpha_8 = 1.95$ and 2.45) respectively. Note that, as in figures 8–10, the red and black curves correspond to $R_\lambda = 550$ and 1067 respectively. The arrowed horizontal line indicates the extent of the scaling range. The vertical arrows indicate the magnitudes of the ratio λ/η at $R_\lambda = 550$ (downward arrow) and 1067 (upward arrow) respectively. Circles correspond to $\overline{(\delta u^*)^6} r^{*-\alpha_6}$ with $\alpha_6 = 1.64$, which is re-estimated from figure 10(*b*) of Anselmet *et al.* (1984) over what we consider to be a more appropriate SR ($50 < r^* < 400$) than that ($20 < r^* < 150$) used in their paper ($R_\lambda = 835$); squares correspond to $\overline{(\delta u^*)^2} r^{*-2/3}$ of Anselmet *et al.* (1984). Also included are $\overline{(\delta u^*)^2} r^{*-2/3}$ and $\overline{(\delta u^*)^3} r^{*-\alpha_3}$ ($\alpha_3 = 0.94$ and 1) at $R_\lambda = 550$ (red) and 1067 (black). Blue and green dashed horizontal lines correspond to 4/5 and 2 respectively.

$r^{4/3}$, for conformity with K41. Therefore, the spectrum $E_p(k_1)$, which corresponds to $D_p(r)$, should behave as $k_1^{-7/3}$ (K41). As mentioned in the Introduction, Tsuji & Ishihara (2003) measured pressure spectra on the centreline of a circular jet over a large range of R_λ (= 200–1250). They found that the $-7/3$ power-law scaling is approached as R_λ increases and actually reached for $R_\lambda \geqslant 600$. In fact, R_λ may need to exceed 1000 if a polynomial fit is applied to the data in figure 4 of Tsuji & Ishihara (2003), see the present figure 12. Using EDQNM simulations in freely decaying homogeneous isotropic turbulence, Meldi & Sagaut (2013) further confirmed the FRN effect on the pressure spectrum and revealed that $R_\lambda \sim 10000$ is needed before a one-decade SR can be observed in the pressure spectrum with a K41 -7/3 scaling. Figure 13 indicates that on the axis of both plane and circular jets a 4/3 power-law scaling, consistent with observations for $E_p(k_1)$ reported in other flows (Tsuji & Ishihara 2003; Meldi & Sagaut 2013), is also approached as R_λ increases, and appears to be confirmed for $R_\lambda \approx 900$ on the axis of the plane jet. Another important aspect of figure 13 is that the distribution of α_4, like that of T_λ in figure 6, differs between the plane jet and circular jet. This difference reflects variations in the

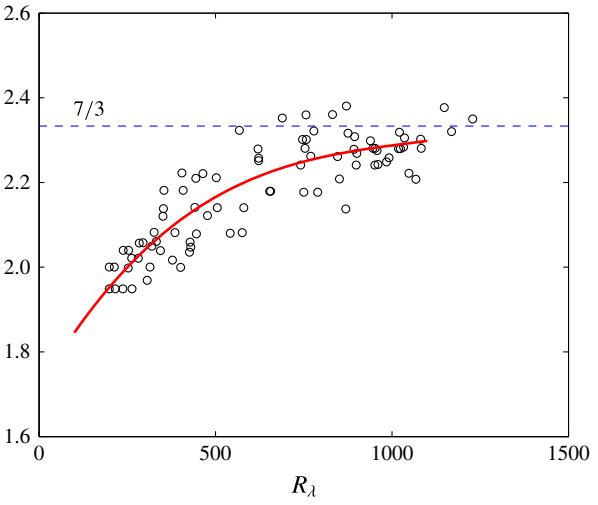

FIGURE 12. (Colour online) Scaling exponents for the pressure spectrum $E_p(k_1)$. Symbols are reproduced from figure 4 of Tsuji & Ishihara (2003). The red curve is a third-order polynomial fit. The dashed line indicates the 7/3 power-law scaling predicted by K41.

contributions from different mechanisms taking place at large scales and vindicates our earlier contention that the way the 4/3 power-law scaling is approached is flow dependent.

Figures 14 and 15 show the variation with R_λ of α_6 and α_8 along the axis of both plane and circular jets. In each flow, α_6 and α_8 increase as R_λ increases. Further, the distributions for both α_6 and α_8 differ between the plane jet and the circular jet. However, the values of 2 and 8/3 predicted by (1.3) for $n=6$ and $n=8$, respectively, are not approached, even for $R_\lambda = 1067$. On the other hand, the magnitudes of α_4, α_6 and α_8 shown in figures 13–15 intersect the predictions by the intermittency model of She & Leveque (1994), log-normal model (K62) and the β-model (Frisch *et al.* 1978) with $\mu = 0.2$, suggesting that it is simply incorrect to use K62 to 'model' the FRN effect. For the present plane jet data ($550 \leqslant R_\lambda \leqslant 1067$), it is almost evident that any uncertainty in the position $r=\lambda$ will not affect any of the results (associated with the FRN effect). It can be seen from figure 11 that, over the SR, the black ($R_\lambda = 1067$) and red ($R_\lambda = 550$) lines are essentially horizontal to each other. The rate of change with R_λ of $\overline{(\delta u^*)^n} r^{*-\alpha_n}$ is therefore unlikely to change across the SR and cannot be affected by the small uncertainty in λ (the error in λ has been included in table 1; the maximum uncertainty is approximately 4 % at the largest R_λ). Figure 11 implies that the FRN effect will be unchanged between $r=\lambda$ and perhaps even beyond $r=5\lambda$ (near the upper end of SR). Finally, the dependence on R_λ of α_n ($n=2-8$) for $R_\lambda = 550$ and 1067 on the axis of the plane jet is shown in figure 16. A number of comments can be made with regard to figure 16.

(i) It is clear that the scaling exponent, for each n, increases noticeably with increasing R_λ. Since the measurements are carried out in the same flow and at the same location, this trend can only be attributed to the FRN effect. This effect can also be seen in Hao *et al.*'s (2008) distributions of the transverse velocity structure functions along the centreline of a wake at $x/d = 75$ when R_λ increases from 120 to 320. These authors reported essentially no R_λ dependence for the SR exponents associated with the longitudinal structure functions. However, these exponents were

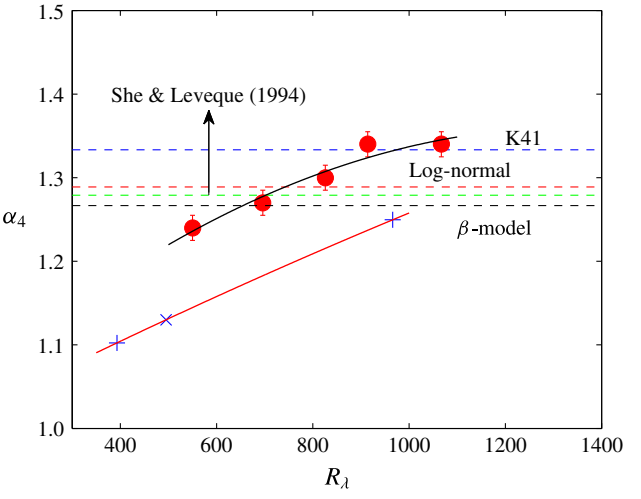

FIGURE 13. (Colour online) Dependence of α_4 on R_λ on the axis of the plane jet (●) and circular jet (+ and × are estimated from Antonia *et al.* (1982*a*) and Pearson & Antonia (2001) respectively, see figure 19 for more details). The blue dashed line indicates the 4/3 power-law scaling predicted by (1.3) with $n = 4$. The red dashed line indicates the log-normal model (K62) $\alpha_n = n/3 - \mu n/18(n-3)$ with $\mu = 0.2$. The black dashed line indicates the β-model (Frisch *et al.* 1978) $\alpha_n = n/3 - \mu/3(n-3)$ with $\mu = 0.2$. The green dashed line indicates the intermittency model of She & Leveque (1994), $\alpha_n = n/9 + 2[1 - (2/3)^{n/3}]$. The black (plane jet) and red (circular jet) curves are second-order polynomial fits.

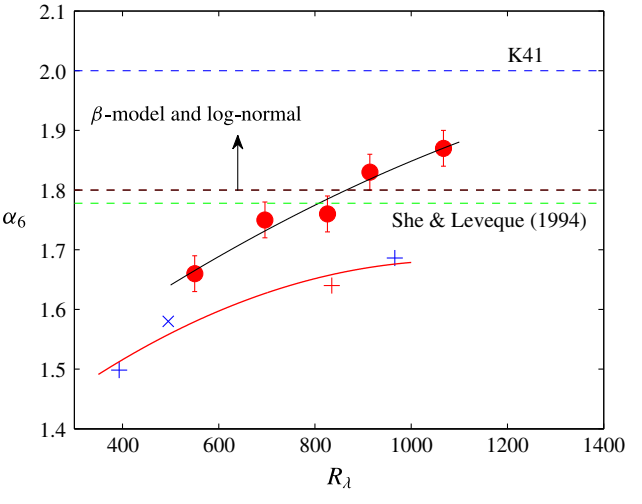

FIGURE 14. (Colour online) Dependence of α_6 on R_λ on the axis of the plane jet. Symbols and lines same as in figure 13; + is estimated from Anselmet *et al.* (1984).

estimated with the extended self-similarity method (ESS) (Benzi *et al.* 1993), which is incorrect for at least two reasons. First, ESS extends the scaling range down to the Kolmogorov scale (Benzi *et al.* 1993), whereas figures 8–11 clearly show that

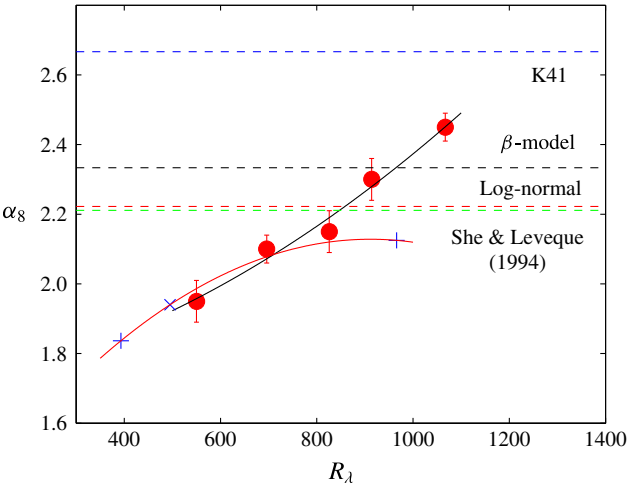

FIGURE 15. (Colour online) Dependence of α_8 on R_λ on the axis of the plane jet. Symbols and lines same as in figure 13.

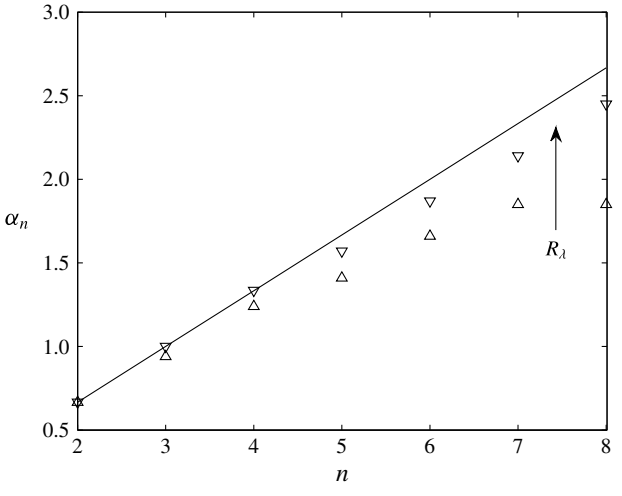

FIGURE 16. Scaling exponents on the axis of the plane jet at $R_\lambda = 550$ ($\triangle$) and 1067 ($\triangledown$). Solid line is the K41 prediction, i.e. $\alpha_n = n/3$, equation (1.3).

SR only starts approximately at $r = \lambda$. Second, the exponents estimated by ESS are relative to $\overline{|\delta u|^3}$ which depends on R_λ (Antonia & Burattini 2006). Figure 17 shows the distributions of $\overline{(\delta u^*)^6}$ as a function of $\overline{|\delta u^*|^3}$ at $R_\lambda = 550$, 696, 826, 914 and 1067 respectively ($\alpha_6 \approx 1.74$ for all cases). Consequently, ESS masks the FRN effect. The FRN effect on the SR scaling exponents of $\overline{(\delta u)^n}$ can also be easily observed from the wake data of Antonia *et al.* (2002*b*) at $x/d = 70$ when R_λ increases from 160 to 280; this will be briefly discussed later (in the context of figure 20).

(ii) For $n > 3$ at a fixed R_λ, the larger n is, the larger is the departure from the $n/3$ (K41) scaling.

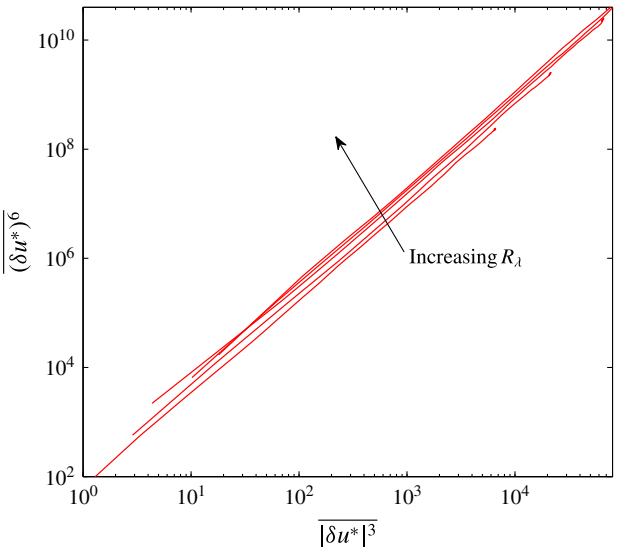

FIGURE 17. (Colour online) Distributions of $\overline{(\delta u^*)^6}$ as a function of $\overline{|\delta u^*|^3}$ on the axis of the plane jet at $R_\lambda = 550$, 696, 826, 914 and 1067; the arrow indicates the direction R_λ increases.

(iii) For $n > 3$, the 'anomalous' scaling, or departure of α_n from $n/3$, decreases as R_λ increases, thus strongly underlining that the FRN effect cannot be ignored.

(iv) The so-called intermittency correction or intermittency exponent μ, when estimated via the autocorrelation function $\overline{\epsilon(x)\epsilon(x+r)} \sim (L/r)^\mu$ (ϵ is the one-dimensional surrogate $\epsilon = 15\nu(\partial u/\partial x)^2$), increases with increasing R_λ before eventually approaching a value of 0.2 at sufficiently large R_λ. Cleve *et al.* (2004) made a compilation of values of μ in various turbulent flows; they are shown in figure 18 without identifying the individual sources. For the flow along the axis of the plane jet, estimates of μ via the autocorrelation function are nearly constant with a value of 0.17 (see also Praskovsky & Oncley 1994), in agreement with the data reported in other flows at large R_λ. Figure 16 (see also figure 14) shows that $2 - \alpha_6$, which has also been identified by many investigators with μ, not only decreases as R_λ increases, but also differs between the plane jet and circular jet at a fixed R_λ. It is worth recalling that Frisch *et al.* (1978) conjectured that $\overline{(\delta u)^6}$ and dissipation correlation function $\overline{\epsilon(x)\epsilon(x+r)}$ are related by

$$\overline{(\delta u)^6}/r^2 \sim \overline{\epsilon(x)\epsilon(x+r)}. \tag{6.2}$$

Clearly, there is an inconsistency between the left- and right-hand sides of (6.2), at least when R_λ is not sufficiently large. It would seem that the use of the right-hand side can lead to a universal value of μ and could be retained for such a purpose. This is perhaps not surprising since ϵ is related to the nearly homogeneous and isotropic small scales, whilst the increment δu, when r lies in the SR, is affected by the inhomogeneous and anisotropic large scales. The left-hand side of (6.2) is therefore affected by the FRN effect and nature of the flow. The trend of our data implies that $\overline{(\delta u)^6}$ (or α_6) could finally go to K41, provided R_λ is sufficiently large;

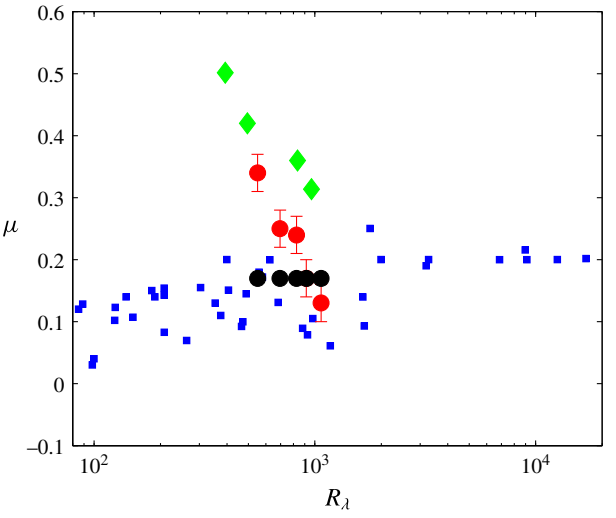

FIGURE 18. (Colour online) Intermittency exponent μ inferred from the autocorrelation function $\overline{\epsilon(x)\epsilon(x+r)}$, ●, along the axis of the plane jet; ■, figure 3 of Cleve *et al.* (2004) without identifying the sources. Values of $2-\alpha_6$ are also shown for the plane jet (●) and circular jet (◆).

in that case, one expects that, just as for $\overline{(\delta u)^3}$, there should be no intermittency correction for $\overline{(\delta u)^6}$; this expectation merits further investigation. In any case, the FRN effect, which depends on the flow, needs to be properly accounted for before one can decide if K41 is valid or whether intermittency corrections to K41, such as introduced by K62, are needed.

Estimates of α_n for $n = 4$, 6, 8 on the axis of the circular jet (from figure 6 of Antonia *et al.* 1982*a*) at $R_\lambda \sim 400$ (these values of α_n are averaged from estimates of α_n at three slightly different values of R_λ (379, 388, 412)) and at $R_\lambda = 966$ are shown in figure 19. Estimates, based on the round jet data of Pearson & Antonia (2001) at $R_\lambda = 485$, are also shown. It is obvious that the trend observed on the axis of the plane jet (figure 16) can also be seen in figure 19. In particular, the magnitude of α_6 at $R_\lambda = 852$, which we have re-estimated from figure 10(*b*) of Anselmet *et al.* (1984) over what we consider to be a more appropriate SR ($50 < r^* < 400$) than that ($20 < r^* < 150$) used in their paper (the compensated $\overline{(\delta u^*)^6} r^{*-\alpha_6}$ with $\alpha_6 = 1.64$ is shown in figure 11), is slightly smaller than that at $R_\lambda = 966$ due to the smaller R_λ in Anselmet *et al.*'s (1984) experiment.

6.2. *Wake and SFPBT*

Further, the FRN effect on α_n on the centreline of a wake at $x/d = 70$ can be also observed in figure 20. Frisch (1995) (section 8.4 of his book) demonstrated that the dependence of even-order exponents α_{2n} on n should be concave based on the Hölder inequality and assuming the existence of such exponents. It can be seen from figure 20 that α_{2n} versus n is convex on the centreline of a wake, implying that the structure functions in the wake do not have a well-defined scaling range. This is not surprising since $R_\lambda (= 160 - 280)$ in the wake is significantly smaller than in the plane and circular jet flows ($R_\lambda = 400 - 1100$). It is nonetheless of interest to include the wake data since the FRN effect on α_n is more emphatically observed in this flow.

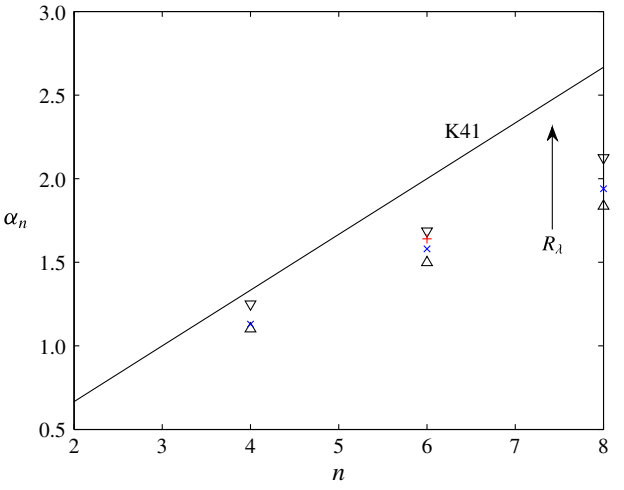

FIGURE 19. (Colour online) Scaling exponents at $R_\lambda \sim 400$ ($\triangle$) and $R_\lambda = 966$ ($\triangledown$) on the axis of the circular jet. They are estimated from figure 6 of Antonia *et al.* (1982*a*). The $+$ is re-estimated from figure 10(*b*) of Anselmet *et al.* (1984) in the SR ($50 < r^* < 400$) at $R_\lambda = 835$; $\times$ are estimated from Pearson & Antonia (2001) at $R_\lambda = 485$. Solid line is the K41 prediction ($\alpha_n = n/3$), equation (1.3).

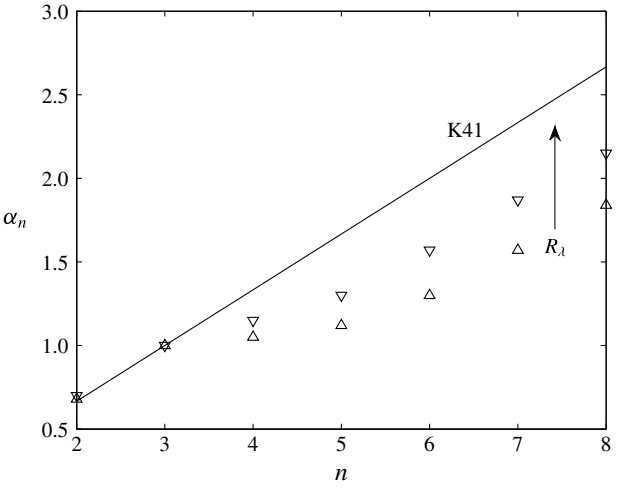

FIGURE 20. Scaling exponents at $R_\lambda = 160$ ($\triangle$) and $R_\lambda = 280$ ($\triangledown$) on the centreline of a circular cylinder wake at $x/d = 70$. They are estimated using the data of Antonia *et al.* (2002*b*). Solid line is the K41 prediction ($\alpha_n = n/3$), equation (1.3).

For SFPBT, Ni & Xia (2013) examined the prefactors of $\overline{(\delta u)^2}$ and the energy spectrum, with the data of Gotoh *et al.* (2002) ($R_\lambda = 70$–460), in the SR. They found that these prefactors depend on R_λ. As discussed in the context of figure 2, $I_u(\lambda^*)$ for SFPBT also shows a dependence on R_λ. However, the weak contribution of $I_u(\lambda^*)$ in the SR suggests that SFPBT is most ideal for examining scaling exponents of $\overline{(\delta u)^3}$. As shown by Moisy *et al.* (1999), Antonia & Burattini (2006), and Gotoh &

Watanabe (2015), $R_\lambda \sim 10^3$ appears to be sufficient for the 4/5 law to be obtained in this flow. For the higher-order SR scaling exponents of $\overline{(\delta u)^n}$ ($n > 3$), Gotoh *et al.* (2002) found that $\alpha_4 = 1.29 \pm 0.03$, $\alpha_6 = 1.77 \pm 0.04$ and $\alpha_8 = 2.17 \pm 0.07$ respectively at $R_\lambda = 460$ ($k_{max}\eta = 0.96$). In a recent paper, Gotoh & Watanabe (2015) obtained $\alpha_4 = 1.320 \pm 0.004$, $\alpha_6 = 1.810 \pm 0.004$ and $\alpha_8 = 2.196 \pm 0.002$; they evaluated these exponents with good accuracy and high mesh resolution at $R_\lambda = 805$ ($k_{max}\eta > 1.4$). The results show an unmistakable FRN effect on α_n for SFPBT. Also, figure 5(b) of Peters *et al.* (2016) shows α_5 both as a function of r^* and R_λ (= 88, 119, 184, 215, 331, 529 and 754 respectively) for SFPBT; the corresponding $\overline{(\delta u^*)^5}$ has been reported by Boschung *et al.* (2016). We can observe from figure 5(b) of Peters *et al.* (2016) that α_5 increases from about 1.50 to 1.56 as R_λ increases from 529 to 754 ($80 < r^* < 250$) although their data appear to show that there is not a distinct SR when $R_\lambda \leqslant 331$ (the α_5 distributions have no discernible plateau). All these results show a FRN effect on α_n for SFPBT, as observed in plane and circular jets and wakes (figures 16, 19–20). However, unlike the plane and circular jets, α_n ($n > 3$) increases at a much slower rate for SFPBT, e.g. α_8 only increases from 2.17 to 2.195 as R_λ increases from 460 to 805. For the plane jet, α_8 increases from 1.95 to 2.16 as R_λ increases from 550 to 826 (see figure 15). Nevertheless, it is clear that figures 19–20 and the data for SFPBT provide further strong support for our contention that the FRN effect must be carefully accounted for.

As pointed out in the Introduction, both K41 and K62 require $R_\lambda \to \infty$. When the Reynolds number is finite one may expect that over the SR, $\overline{(\delta u^*)^n}$ can be expressed as (1.5) In this section, we have shown that, for $n > 3$, the tendency is for α_n to increase. It is as yet unclear whether α_n will approach the value of $n/3$ as predicted by K41 or whether it will continue to depend on R_λ. In § 5, it was found that C_{un}^{FRN}, for $n = 3$, also approaches the K41 constant (i.e. 4/5) although the way this constant is approached is flow dependent. For $n > 3$, K41 do not predict exact values for C_{un}. However, it can be seen from figure 11 that $C_{un}^{FRN} (= \overline{(\delta u^*)^n} r^{*-\alpha_n})$ for $n > 3$ also depends on R_λ. It is worth recalling that all flows considered here (along the axis in the far field of circular & plane jets, grid turbulence, etc.) fall in the 'energy equilibrium' group, in the sense used by Valente & Vassilicos (2012), Hearst & Lavoie (2014), Vassilicos (2015), Obligado, Dairay & Vassilicos (2016). In the near-field region of a cylinder wake, jet and grid turbulence (see for example Valente & Vassilicos 2012; Hearst & Lavoie 2014; Vassilicos 2015; Obligado *et al.* 2016), several large-scale effects may coexist (production due to mean shear, production due to interactions between coherent motions, turbulent/pressure diffusion and so on) thus leading to non-equilibrium flows. It is expected that these large-scale effects will affect the behaviour of the velocity structure functions since they contribute to the FRN effect.

7. Concluding discussion

The effect of the large-scale forcing on $\overline{(\delta u^*)^n}$ ($n = 2$, 3) at $r = \lambda$ has been assessed in various turbulent flows at small to moderate R_λ. We have focused on $r = \lambda$ since this separation is sufficiently large to be at the lower end of the SR and, perhaps more importantly, it is located near where the normalized transfer of energy, i.e. $-\overline{(\delta u^*)^3}$ is maximum. The section $r = \lambda$ provides an appropriate means of quantifying the influence of the inhomogeneous term $I_u(r)$ (see § 4) on $\overline{(\delta u^*)^n}$ ($n = 2$, 3) especially since the departure from local isotropy (figure 1) at $r = \lambda$ is reasonably small. The results show that the contribution of $I_u(r)$ to the scale by scale energy budget differs

from flow to flow. For a fixed R_λ, the contribution is largest on the centreline of a fully developed channel flow and smallest for SFPBT. For decaying-type flows, the contribution lies between these two cases. Because of the difference in $I_u(r)$ in each flow, T_λ $(=-\overline{(\delta u^*)^3}_{r=\lambda})$ differs from flow to flow over the range of R_λ covered in this study although its effect on $\overline{(\delta u^*)^2}$ at $r=\lambda$ appears to be negligible.

The FRN effect on the SR scaling exponents of $\overline{(\delta u)^n}$ has been examined using measurements of u at moderately large R_λ $(=500$–$1100)$ on the axis of a plane jet. The main feature of figures 13–15, 16, 19 and 20 is that the magnitude of α_n depends not only on R_λ, but also on the flow. This behaviour suggests that the FRN effect needs to be properly accounted for before making meaningful assessments with regard to K41 and K62. Both K41 and K62 require local homogeneity and isotropy and R_λ to be very large. We have underlined in various sections of the text that it is imprudent, if not incorrect, to associate the FRN effect with a consequence of K62 (1.4). We believe that this association has misled the vast majority of post 1962 studies; as a result, K41 has by and large been abandoned in favour of K62.

We should also stress that (6.1) is derived from the Navier–Stokes equations. Namely, in the SR, if the fourth-order velocity structure function $D_{1111}(r)$ $(=\overline{(\delta u)^4})$ varies as $r^{4/3}$, $E_p(k_1)$ should vary as $k_1^{-7/3}$ for conformity with K41 at large R_λ (the former is confirmed by the results on the axis of the plane jet and the latter by Tsuji & Ishihara (2003) and Meldi & Sagaut (2013)), whereas the SR scaling exponents for both $E_p(k_1)$ and $\overline{(\delta u)^4}$ depend on R_λ at small to moderate R_λ. We should also note that the FRN effect on the statistical properties of the dissipation scales is also observed in various turbulent flows. For example, Tang *et al.* (2015*a*), Antonia *et al.* (2015), Tang *et al.* (2015*b*) showed that the FRN effect on the velocity derivative skewness S can be recast in the form C/R_λ (C is a constant which differs from flow to flow, e.g. along the axis in the far field of an axisymmetric jet flow, $C=90/[7(2+R)]$, where $R=\overline{v^2}/\overline{u^2}$ (Antonia *et al.* 2015)). The present work extends in an important way the work reported in previous papers which focused primarily on the dissipative scales and showed that the first similarity hypothesis in K41, albeit with some important relaxations (R_λ does not in fact need to be very large nor is local isotropy strictly necessary), was satisfied quite adequately. Here, the emphasis has been on statistics associated with the SR. Evidently, much higher values of R_λ are needed before the FRN effect on the SR scales disappears. When the IR is eventually established, one cannot yet rule out that the skewness of δu will approach a constant as predicted by K41 and supported by our analysis in § 4. The results of figures 13–15, 16, 19 and 20 strongly underline the fact that insufficient attention has been given in the past to the FRN effect on the SR and, in particular, the possibility that this effect only becomes more pronounced as the order of the structure function increases. The deviation of α_n from K41 obtained by Anselmet *et al.* (1984), a paper which was influential in terms of providing strong support for the departure from K41, needs to be reappraised critically in the light of the present results. It is pertinent to recall here that when $R_\lambda \to \infty$, I_u should become negligible across the IR and (1.1) becomes an accurate simplification of (1.2). Note that (1.1) is satisfied by K41 in a natural way whereas any intermittency model used in conjunction with K62 must be chosen so as to comply with the '4/5' law.

Finally, it would be desirable to further confirm the present observations of the FRN effect in other types of flows such as non-equilibrium flows(Valente & Vassilicos 2012; Hearst & Lavoie 2014; Vassilicos 2015), wall shear flows or the so-called French washing machine (Tabeling *et al.* 1996; Belin *et al.* 1997) which can provide larger

Reynolds numbers than in this study. Evidently, the major challenge will continue to be the attainment of sufficiently high Reynolds numbers to allow the influence of I_u on the SR to be reduced considerably and therefore provide appropriate conditions, e.g. local homogeneity and isotropy, for testing K41 (especially the second similarity hypothesis) and K62 with much less ambiguity than in the past.

Acknowledgements

The financial support of the Australian Research Council (ARC) is gratefully acknowledged. Y.Z. wishes to acknowledge support given to him from Scientific Research Fund of Shenzhen Government through grant JCYJ20140417172417119 and NSFC through grant 11632006. The National Research Foundation for the Doctoral Program of Higher Education of China under Grant No. 20132302110054 is acknowledged.

REFERENCES

ANSELMET, F., GAGNE, Y., HOPFINGER, E. J. & ANTONIA, R. A. 1984 High-order velocity structure functions in turbulent shear flows. *J. Fluid Mech.* **140**, 63–89.

ANTONIA, R. A. & BURATTINI, P. 2006 Approach to the 4/5 law in homogeneous isotropic turbulence. *J. Fluid Mech.* **550**, 175–184.

ANTONIA, R. A., DJENIDI, L. & DANAILA, L. 2014 Collapse of the turbulent dissipation range on kolmogorov scales. *Phys. Fluids* **26**, 045105.

ANTONIA, R. A. & PEARSON, B. R. 2000 Reynolds number dependence of velocity structure functions in a turbulent pipe flow. *Flow Turbul. Combust.* **64**, 95–117.

ANTONIA, R. A., PEARSON, B. R. & ZHOU, T. 2000*a* Reynolds number dependence of second-order velocity structure functions. *Phys. Fluids* **12**, 3000–3006.

ANTONIA, R. A., PEARSON, B. R. & ZHOU, T. 2002*a* Reynolds number dependence of second-order velocity structure functions. *Phys. Fluids* **12**, 3000–3006.

ANTONIA, R. A., SATYAPRAKASH, B. R. & CHAMBERS, A. J. 1982*a* Reynolds number dependence of velocity structure functions in turbulent shear flows. *Phys. Fluids* **25**, 29–37.

ANTONIA, R. A., SATYAPRAKASH, B. R. & HUSSAIN, A. K. M. F. 1982*b* Statistics of fine-scale velocity in turbulent plane and circular jets. *J. Fluid Mech.* **119**, 55–89.

ANTONIA, R. A., SMALLEY, R. J., ZHOU, T., ANSELMET, F. & DANAILA, L. 2003 Similarity of energy structure functions in decaying homogeneous isotropic turbulence. *J. Fluid Mech.* **487**, 245–269.

ANTONIA, R. A., TANG, S. L., DJENIDI, L. & DANAILA, L. 2015 Boundedness of the velocity derivative skewness in various turbulent flows. *J. Fluid Mech.* **781**, 727–744.

ANTONIA, R. A., ZHOU, T., DANAILA, L. & ANSELMET, F. 2000*b* Streamwise inhomogeneity of decaying grid turbulence. *Phys. Fluids* **12**, 3086–3089.

ANTONIA, R. A., ZHOU, T. & ROMANO, G. P. 2002*b* Small-scale turbulence characteristics of two-dimensional bluff body wakes. *J. Fluid Mech.* **459**, 67–92.

BATCHELOR, G. K. 1951 Pressure fluctuations in isotropic turbulence. *Proc. Camb. Phil. Soc.* **47**, 533–559.

BELIN, F., MAURER, J., TABELING, P. & WILLAIME, H. 1997 Velocity gradient distributions in fully developed turbulence: experimental study. *Phys. Fluids* **9**, 3843–3850.

BENZI, R., CILIBERTO, S., TRIPICCIONE, R., BAUDET, C., MASSAIOLI, F. & SUCCI, S. 1993 Extended self-similarity in turbulent flows. *Phys. Rev.* E **48**, 29–32.

BOS, W. J. T., CHEVILLARD, L., SCOTT, J. F. & RUBINSTEIN, R. 2012 Reynolds number effect on the velocity increment skewness in isotropic turbulence. *Phys. Fluids* **24**, 015108.

BOSCHUNG, J., HENNIG, F., GAUDING, M., PITSCH, H. & PETERS, N. 2016 Generalised higher-order Kolmogorov scales. *J. Fluid Mech.* **794**, 233–251.

BURATTINI, P., ANTONIA, R. A. & DANAILA, L. 2005*a* Scale-by-scale energy budget on the axis of a turbulent round jet. *J. Turbul.* **6**, N19.

BURATTINI, P., ANTONIA, R. A. & DANAILA, L. 2005*b* Similarity in the far field of a turbulent round jet. *Phys. Fluids* **17**, 025101.

CLEVE, J., GREINER, M., PEARSON, B. R. & SREENIVASAN, K. R. 2004 Intermittency exponent of the turbulent energy cascade. *Phys. Rev.* E **69**, 066316.

DANAILA, L., ANSELMET, F. & ANTONIA, R. A. 2002 An overview of the effect of large-scale inhomogeneities on small-scale turbulence. *Phys. Fluids* **14**, 2475–2482.

DANAILA, L., ANSELMET, F., ZHOU, T. & ANTONIA, R. A. 1999 A generalization of Yaglom's equation which accounts for the large-scale forcing in heated decaying turbulence. *J. Fluid Mech.* **391**, 359–372.

DANAILA, L., ANSELMET, F., ZHOU, T. & ANTONIA, R. A. 2001 Turbulent energy scale-budget equations in a fully developed channel flow. *J. Fluid Mech.* **430**, 87–109.

DANAILA, L., ANTONIA, R. A. & BURATTINI, P. 2004 Progress in studying small-scale turbulence using 'exact' two-point equations. *New J. Phys.* **6**, 2–23.

DJENIDI, L. & ANTONIA, R. A. 2015 A general self-preservation analysis for decaying homogenous isotropic turbulence. *J. Fluid Mech.* **773**, 345–365.

FRISCH, U. 1995 *Turbulence: The Legacy of A. N. Kolmogorov*. Cambridge University Press.

FRISCH, U., SULEM, P. L. & NELKIN, M. 1978 A simple dynamical model of intermittent fully developed turbulence. *J. Fluid Mech.* **87**, 719–736.

FUKAYAMA, D., OYAMADA, T., NAKANO, T., GOTOH, T. & YAMAMOTO, K. 2000 Longitudinal structure functions in decaying and forced turbulence. *J. Phys. Soc. Japan* **69**, 701–715.

GOTOH, T., FUKAYAMA, D. & NAKANO, T. 2002 Velocity field statistics in homogeneous steady turbulence obtained using a high-resolution direct numerical simulation. *Phys. Fluids* **14**, 1065–1081.

GOTOH, T. & NAKANO, T. 2003 Role of pressure in turbulence. *J. Stat. Phys.* **113** (5), 855–874.

GOTOH, T. & WATANABE, T. 2015 Power and nonpower laws of passive scalar moments convected by isotropic turbulence. *Phys. Rev. Lett.* **115** (11), 114502.

HAO, Z., ZHOU, T., ZHOU, Y. & MI, J. 2008 Reynolds number dependence of the inertial range scaling of energy dissipation rate and enstrophy in a cylinder wake. *Exp. Fluids* **44**, 279–289.

HEARST, R. J. & LAVOIE, P. 2014 Decay of turbulence generated by a square-fractal-element grid. *J. Fluid Mech.* **741**, 567–584.

HILL, R. J. 2001 Equations relating structure functions of all orders. *J. Fluid Mech.* **434**, 379–388.

HILL, R. J. & WILCZAK, J. M. 1995 Pressure structure functions and spectra for locally isotropic turbulence. *J. Fluid Mech.* **296**, 247–269.

ISHIHARA, T., MORISHITA, K., YOKOKAWA, M., UNO, A. & KANEDA, Y. 2016 Energy spectrum in high-resolution direct numerical simulations of turbulence. *Phys. Rev. Fluids* **1** (8), 082403.

KOLMOGOROV, A. N. 1941*a* Local structure of turbulence in an incompressible fluid for very large Reynolds numbers. *Dokl. Akad. Nauk SSSR* **30**, 299–303.

KOLMOGOROV, A. N. 1941*b* Dissipation of energy in the locally isotropic turbulence. *Dokl. Akad. Nauk SSSR* **32**, 19–21.

KOLMOGOROV, A. N. 1962 A refinement of previous hypotheses concerning the local structure of turbulence in a viscous incompressible fluid at high Reynolds number. *J. Fluid Mech.* **13**, 82–85.

KURIEN, S. & SREENIVASAN, K. R. 2000 Anisotropic scaling contributions to high-order structure functions in high-Reynolds-number turbulence. *Phys. Rev.* E **62**, 2206–2212.

LINDBORG, E. 1999 Correction to the four-fifths law due to variations of the dissipation. *Phys. Fluids* **11**, 510.

L'VOV, V. S. & PROCACCIA, I. 1995 'Intermittency' in hydrodynamic turbulence as intermediate asymptotics to Kolmogorov scaling. *Phys. Rev. Lett.* **74**, 2690.

MAURER, J., TABELING, P. & ZOCCHI, G. 1994 Statistics of turbulence between two counterrotating disks in low-temperature helium gas. *Europhys. Lett.* **26** (1), 31.

MELDI, M. & SAGAUT, P. 2013 Pressure statistics in self-similar freely decaying isotropic turbulence. *J. Fluid Mech.* **717**, R2.

MI, J., XU, M. & ZHOU, T. 2013 Reynolds number influence on statistical behaviors of turbulence in a circular free jet. *Phys. Fluids* **25**, 075101.

MOISY, F., TABELING, P. & WILLAIME, H. 1999 Kolmogorov equation in a fully developed turbulence experiment. *Phys. Rev. Lett.* **82** (20), 3994.

MONIN, A. S. & YAGLOM, A. M. 2007 *Statistical Fluid Dynamics*, vol. 2. MIT.

MORRISON, J. F., VALLIKIVI, M. & SMITS, A. J. 2016 The inertial subrange in turbulent pipe flow: centreline. *J. Fluid Mech.* **788**, 602–613.

MYDLARSKI, L. & WARHAFT, Z. 1996 On the onset of high- Reynolds-number grid-generated wind tunnel turbulence. *J. Fluid Mech.* **320**, 331–368.

NI, R. & XIA, K. Q. 2013 Kolmogorov constants for the second-order structure function and the energy spectrum. *Phys. Rev.* E **87** (2), 023002.

OBLIGADO, M., DAIRAY, T. & VASSILICOS, J. C. 2016 Nonequilibrium scalings of turbulent wakes. *Phys. Rev. Fluids* **1** (4), 044409.

PEARSON, B. R. & ANTONIA, R. A. 2001 Reynolds-number dependence of turbulent velocity and pressure increments. *J. Fluid Mech.* **444**, 343–382.

PETERS, N., BOSCHUNG, J., GAUDING, M., GOEBBERT, J. H., HILL, R. J. & PITSCH, H. 2016 Higher-order dissipation in the theory of homogeneous isotropic turbulence. *J. Fluid Mech.* **803**, 250–274.

POPE, S. B. 2000 *Turbulent Flows*. Cambridge University Press.

PRASKOVSKY, A. & ONCLEY, S. 1994 Measurements of the Kolmogorov constant and intermittency exponent at very high Reynolds numbers. *Phys. Fluids* **6**, 2886–2888.

QIAN, J. 1997 Inertial range and the finite Reynolds number effect of turbulence. *Phys. Rev.* E **55**, 337–342.

QIAN, J. 1998 Normal and anomalous scaling of turbulence. *Phys. Rev.* E **58**, 7325.

QIAN, J. 1999 Slow decay of the finite Reynolds number effect of turbulence. *Phys. Rev.* E **60**, 3409.

SAGAUT, P. & CAMBON, C. 2008 *Homogeneous Turbulence Dynamics*. Cambridge University Press.

SHE, Z.-S. & LEVEQUE, E. 1994 Universal scaling laws in fully developed turbulence. *Phys. Rev. Lett.* **72** (3), 336.

SREENIVASAN, K. & ANTONIA, R. A. 1997 The phenomenology of small-scale turbulence. *Annu. Rev. Fluid Mech.* **29**, 435–472.

TABELING, P., ZOCCHI, G., BELIN, F., MAURER, J. & WILLAIME, H. 1996 Probability density functions, skewness, and flatness in large Reynolds number turbulence. *Phys. Rev.* E **53**, 1613–1621.

TANG, S. L., ANTONIA, R. A., DJENIDI, L., ABE, H., ZHOU, T., DANAILA, L. & ZHOU, Y. 2015*a* Transport equation for the mean turbulent energy dissipation rate on the centreline of a fully developed channel flow. *J. Fluid Mech.* **777**, 151–177.

TANG, S. L., ANTONIA, R. A., DJENIDI, L. & ZHOU, Y. 2015*b* Transport equation for the isotropic turbulent energy dissipation rate in the far-wake of a circular cylinder. *J. Fluid Mech.* **784**, 109–129.

TCHOUFAG, J., SAGAUT, P. & CAMBON, C. 2012 Spectral approach to finite Reynolds number effects on Kolmogorov's 4/5 law in isotropic turbulence. *Phys. Fluids* **24** (1), 015107.

THIESSET, F., ANTONIA, R. A. & DANAILA, L. 2013*b* Scale-by-scale turbulent energy budget in the intermediate wake of two-dimensional generators. *Phys. Fluids* **25**, 115105.

THIESSET, F., ANTONIA, R. A. & DJENIDI, L. 2014 Consequences of self-preservation on the axis of a turbulent round jet. *J. Fluid Mech.* **748**, R2.

THIESSET, F., DANAILA, L. & ANTONIA, R. A. 2013*a* Dynamical effect of the total strain induced by the coherent motion on local isotropy in a wake. *J. Fluid Mech.* **720**, 393–423.

TSUJI, Y. & ISHIHARA, T. 2003 Similarity scaling of pressure fluctuation in turbulence. *Phys. Rev.* E **68**, 026309.

VALENTE, P. C. & VASSILICOS, J. C. 2012 Universal dissipation scaling for non-equilibrium turbulence. *Phys. Rev. Lett.* **108**, 214503.

VASSILICOS, J. C. 2015 Dissipation in turbulent flows. *Annu. Rev. Fluid Mech.* **47**, 95–114.

VEDULA, P. & YEUNG, P. K. 1999 Similarity scaling of acceleration and pressure statistics in numerical simulations of isotropic turbulence. *Phys. Fluids* **11**, 1208–1220.

VINCENT, A. & MENEGUZZI, M. 1991 The spatial structure and statistical properties of homogeneous turbulence. *J. Fluid Mech.* **225**, 1–20.

XU, G., ANTONIA, R. A. & RAJAGOPALAN, S. 2001 Sweeping decorrelation hypothesis in a turbulent round jet. *Fluid Dyn. Res.* **28** (5), 311–321.

ZHOU, T. & ANTONIA, R. A. 2000 Reynolds number dependence of the small-scale structure of grid turbulence. *J. Fluid Mech.* **406**, 81–107.

ZHOU, T., ANTONIA, R. A. & CHUA, L. P. 2005 Flow and Reynolds number dependencies of one-dimensional vorticity fluctuations. *J. Turbul.* **6**, N28.